# Distinct Nrf2 Signaling Thresholds Mediate Lung Tumor Initiation and Progression

Janine M. DeBlasi[1,2], Aimee Falzone[1], Samantha Caldwell[1], Nicolas Prieto-Farigua[1], Justin R. Prigge[3], Edward E. Schmidt[3], Iok In Christine Chio[4,5], Florian A. Karreth[6], Gina M. DeNicola[1*]

[1]Department of Metabolism & Physiology, H. Lee Moffitt Cancer Center and Research Institute, Tampa, FL, 33612, USA.

[2]Cancer Biology PhD Program, University of South Florida, Tampa, FL 33612, USA.

[3]Microbiology & Cell Biology Department, Montana State University, Bozeman, MT 59717, USA.

[4]Institute for Cancer Genetics, Department of Genetics and Development, Columbia University Irving Medical Center, New York, NY 10032, USA.

[5]Herbert Irving Comprehensive Cancer Center, Columbia University Irving Medical Center, New York, NY 10032, USA.

[6]Department of Molecular Oncology, H. Lee Moffitt Cancer Center and Research Institute, Tampa, FL, 33612, USA.

Running Title: Nrf2 Thresholds in Tumor Initiation and Progression

*Correspondence: Gina M. DeNicola, H. Lee Moffitt Cancer Center, 12902 USF Magnolia Dr. SRB3 DeNicola Lab, Tampa FL 33612; Tel: 813-745-8371; email: Gina.DeNicola@moffitt.org

Conflict of interest statement: The authors declare no competing interests.

## ABSTRACT

Mutations in the KEAP1-NRF2 pathway occur in up to a third of non-small cell lung cancer (NSCLC) cases and often confer resistance to therapy and poor outcomes. Here, we developed murine alleles of the KEAP1 and NRF2 mutations found in human NSCLC and comprehensively interrogated their impact on tumor initiation and progression. Chronic Nrf2 stabilization by Keap1 or Nrf2 mutation was not sufficient to induce tumorigenesis, even in the absence of tumor suppressors p53 or Lkb1. When combined with $Kras^{G12D/+}$, constitutive Nrf2 activation promoted lung tumor initiation and early progression of hyperplasia to low-grade tumors but impaired their progression to advanced-grade tumors, which was reversed by Nrf2 deletion. Finally, NRF2 overexpression in KEAP1 mutant NSCLC cell lines was detrimental to cell proliferation, viability, and anchorage-independent colony formation. Collectively, our results establish the context-dependence and activity threshold for NRF2 during the lung tumorigenic process.

**Significance:** This study reports murine lung cancer models harboring mutations in the Keap1/Nrf2 pathway and highlights the context-dependent and diverse roles of Nrf2 during lung tumor initiation and progression.


## Introduction

NRF2 (nuclear factor-erythroid 2 p45-related factor 2) is a stress-responsive transcription factor that regulates the detoxification of reactive oxygen species (ROS), maintains cellular homeostasis, and regulates many facets of metabolism (1, 2). NRF2 is negatively regulated by KEAP1 (Kelch-like ECH-associated protein 1), a substrate adaptor protein for the cullin 3 (CUL3)-based E3 ubiquitin ligase that facilitates NRF2 ubiquitination and proteasomal degradation in the absence of oxidative or xenobiotic stress (3). NRF2 promotes the detoxification of carcinogens to limit deleterious mutations that initiate cancer(4-7) and NRF2 activators are being explored as chemopreventative agents (8-10). However, NRF2 is frequently stabilized in many cancers, particularly non-small cell lung cancer (NSCLC), where

53 mutations in the KEAP1-NRF2 pathway are found in up to 30% of cases (11, 12). NRF2 stabilization is
54 associated with poor prognosis (13-20), resistance to chemo- and radiotherapy (21, 22), cancer cell
55 survival (22), proliferation (23), metabolic reprogramming (20, 24-26), and metastasis (27). It remains
56 unclear, however, whether chronic NRF2 stabilization transforms normal cells. Thus, it is important to
57 understand the contexts and mechanisms by which NRF2 can prevent and promote cancer phenotypes.

58

59 Preclinical genetically engineered mouse models (GEMMs) have advanced our understanding of the role
60 of NRF2 in lung tumorigenesis (23, 27-37). NRF2 activation in NSCLC has been modeled in GEMMs by
61 inactivating Keap1 via conditional knockout (28-31, 33, 35) or CRISPR-mediated deletion (27, 34, 36, 37),
62 in contrast to the KEAP1 mutations found in human lung cancer. These studies have shown that Nrf2
63 promotes lung tumor initiation (29, 30), tumor size (34, 38), progression (33, 34), and metastasis (27).
64 However, other studies have failed to see an effect of Nrf2 on lung tumor initiation (38, 39) or size (36, 37,
65 39), and we reported that Nrf2 activation significantly decreases tumor size (32). Study conditions, time
66 points and phenotypes assayed varied across these studies. Therefore, the role NRF2 activation plays at
67 distinct stages of tumor initiation and progression remains to be determined.

68

69 In the current study, we generated lung cancer GEMMs expressing Keap1$^{R554Q}$ and Nrf2$^{D29H}$ mutations to
70 comprehensively investigate how Nrf2 activation affects each stage of the tumorigenic process. These
71 models also exhibit a series of graded NRF2 activation, allowing us to ask how different levels of Nrf2
72 influence lung tumor progression. We found that constitutive Nrf2 stabilization induced by these mutations
73 was insufficient for lung tumor development, even in the context of tumor suppressor loss. In contrast,
74 these mutations promoted lung tumor initiation in the Kras$^{G12D/+}$ model of early lung adenocarcinoma,
75 consistent with previous studies (23, 29, 30).

76

77 Using the Kras$^{G12D/+}$; p53$^{fl/fl}$ adenocarcinoma model, we found that homozygous Keap1 mutation
78 unexpectedly blocked tumor progression. Supportingly, we found that Nrf2 expression and activity was
79 downregulated in advanced tumors, and Nrf2 deletion could rescue the Keap1 mutation-mediated

progression impairment. Overall, our data suggest that NRF2 has distinct, threshold-dependent effects during lung tumor initiation and progression.

## Materials and Methods

### Lead contact

Further information and requests for resources and reagents should be directed to and will be fulfilled by the Lead Contact, Dr. Gina M. DeNicola (Gina.DeNicola@moffitt.org).

### Material availability

All unique reagents generated in this study are available from the Lead Contact without restriction.

### Mice

Mice were housed and bred in accordance with the ethical regulations and approval of the IACUC (protocols #: IS00003893R and IS00007922R). Generation of the Keap1 targeting vector was previously described (32). Briefly, the *CA-Keap1*$^{R554Q}$ allele (Keap1$^{tm1Gmdn}$, MGI: 7327097) was made by inserting a wild-type *Keap1* cDNA containing exons 3-5 flanked by loxP sites upstream of the R554Q mutation in exon 4 of the *Keap1* gene. *Keap1* was targeted in C10 murine ES cells and cells were selected with blasticidin. To make the *LSL-Nfe2l2*$^{D29H}$ allele (Nfe2l2$^{tm1Gmdn}$, MGI: 7327101), a STOP cassette flanked by loxP sites was inserted into intron 1 and codon 29 in endogenous exon 2 was mutated from an aspartic acid to a histidine. The endogenous *Nfe2l2* locus was targeted in C10 murine ES cells and puromycin was used to select positive cells. For both alleles, positive clones were screened by copy number real-time PCR and injected into blastocysts. Genotyping primers were as follows: for the *Keap1*$^{R554Q}$ allele: Mutant forward: 5'-ATGGCCACACTTTTCTGGAC-3'; wild-type (WT) forward: 5'-GGGGGTAGAGGGAGGAGAAT-3'; Common reverse: 5'-GCCACCCTATTCACAGACCA-3'. The WT PCR product was 326 bp and the mutant PCR product 584 bp. For the *Nfe2l2*$^{D29H}$ allele: WT forward: 5'-

105 GAGGCAGGTAGTTCTCTGAGTTTG-3'; Common reverse: 5'-GCAAATGCACTGAGACACTCAT-3';
106 Mutant forward: 5'-CTAGCCACCATGGCTTGAGT-3'. The WT PCR product was 189 bp and the mutant
107 PCR product 282 bp. All mice were maintained on a mixed C57BL/6 genetic background. In addition to
108 Keap1$^{R554Q}$ and Nrf2$^{D29H}$ mice, p53$^{flox}$ (RRID:IMSR_JAX:008462); Lkb1$^{flox}$ (RRID:IMSR_JAX:014143);
109 Nrf2$^{flox}$ (RRID:IMSR_JAX:025433); and LSL-Kras$^{G12D/+}$ (RRID:IMSR_JAX:008179) mice were used. For
110 mouse lung tumor studies, intranasal installation of 2.5 x $10^7$ PFU adenoviral-Cre (University of Iowa) was
111 used to induce lung tumors as previously described (40). Adenoviral infections were performed under
112 isofluorane anesthesia.

113

114 **Murine embryonic fibroblast generation and culture**

115 MEFs were isolated from E13.5-14.5-day old embryos and maintained in pyruvate-free DMEM (Corning)
116 containing 10% FBS, 100 units/mL penicillin and 100 µg/mL streptomycin (Gibco) in a humidified
117 incubator with 5% $CO_2$ and 95% air at 37°C. MEFs were used within four passages and infected with
118 control empty adenovirus or adenoviral-Cre (University of Iowa) at an approximate multiplicity of infection
119 of 500.

120

121 **RNA-sequencing preparation and analysis**

122 Samples were prepared using the RNeasy plus mini kit (Qiagen, 74134). RNA quality was checked with
123 the QIAxcel RNA QC kit (Qiagen, 929104). Additional RNA QC, sequencing, mapping to the mouse
124 genome, and analysis were performed by Novogene. Differentially expressed genes (DESeq2) with $p <$
125 $0.05$ were included in the volcano plot.

126

127 **Immunohistochemistry (IHC)**

128 Mouse lung tissue was fixed with 10% formalin overnight, transferred to 70% ethanol and paraffin
129 embedded to be sectioned. Unstained tissue sections were de-paraffinized in xylene followed by
130 rehydration in a graded alcohol series. Antigen retrieval was performed by boiling in 10mM citrate buffer

131 (pH 6). Antibodies used for IHC include affinity-purified NRF2 (1:150 or 1:300) (41), NQO1 (Sigma
132 Aldrich, RRID:AB_1079501, 1:500), Ki-67 (Cell Signaling Technology, RRID:AB_2620142, 1:200), and
133 Cleaved Caspase-3 (Cell Signaling Technology, RRID:AB_2070042, 1:1000). Following overnight
134 incubation at 4°C in primary antibody, the ImmPRESS HRP goat anti-rabbit kit (Vector Laboratories,
135 RRID:AB_2631198) was used as directed by manufacturer's instructions. DAB peroxidase (HRP)
136 substrate (Vector Laboratories, SK-4105) was used to develop immunohistochemical staining, followed
137 by counterstaining with hematoxylin (Vector Laboratories, H-3404). Slides were scanned with the Aperio
138 imager at 20x and the H-score of at least five representative regions/ mouse was analyzed with QuPath
139 software(42). Representative images were captured using the Axio Lab.A1 microscope at 40x (Carl Zeiss
140 Microimaging Inc.).

141

142 **Tumor grading analysis and histology**

143 Lung tumor grading was performed manually as previously described (43). Tumor grading distribution
144 percentages were calculated by dividing the number of tumors in a specific grade by the total number of
145 tumors per mouse. Tumor burden by grade was calculated by dividing the area of the lung covered by a
146 specific tumor grade by the total lung area.

147

148 **NSCLC cell lines and culture**

149 Human lung cancer cell lines used include H1944 (RRID:CVCL_1508), H322 (RRID:CVCL_1556), A549
150 (RRID:CVCL_0023), HCC15 (RRID:CVCL_2057), and H460 (RRID:CVCL_0459) and were previously
151 described (24). All cell lines were acquired from an authentic source (Hamon Cancer Center Collection).
152 Cells were cultured in RPMI 1640 (Gibco) containing 5% FBS without antibiotics in a humidified incubator
153 with 5% $CO_2$ and 95% air at 37°C. Cells were confirmed to be free of mycoplasma with the MycoAlert kit
154 (Lonza) immediately upon receipt and aliquots were frozen. Cell lines were tested monthly for
155 mycoplasma and used within 10-20 passages.

156

157 **Lentivirus generation and infection of NSCLC cells**

158 Lentiviruses were made by transfecting Lenti-X 293T cells (Takara 632180) overnight with
159 polyethylenimine (PEI), lentiviral plasmid (pLX317-NRF2(44) or the control pLX317 empty vector(32)),
160 and packaging plasmids pCMV-dR8.2 dvpr (RRID:Addgene_8455) and pCMV-VSV-G
161 (RRID:Addgene_8454) in DMEM containing 10% FBS. To generate NRF2-overexpressing cells, NSCLC
162 cells were transduced for 24 hrs with lentiviruses in medium containing polybrene (8 µg/mL). After
163 transduction, infected cells were selected with 0.5 µg/mL (H1944, H322, H460) or 1 µg/mL (A549,
164 HCC15) puromycin for 72 hrs. Immediately following selection, cells were seeded in respective puromycin
165 concentrations for the indicated assays.

166

167 **Cell proliferation and cell death assays**

168 NSCLC cells were monitored with the CELLCYTE X™ live cell imaging instrument (Cytena) over the
169 course of 96 hours. Prior to imaging, SYTOX Green nucleic acid stain (Thermo Fisher Scientific, S7020)
170 was added to medium at a final concentration of 20 nM. Images were acquired from each well at 8-hour
171 intervals and analyzed using CellCyte Studio (CELLINK). Cell confluency was represented as the % of
172 the image covered by cells. The number of dead cells was normalized to cell confluency [number of Sytox
173 Green positive cells/ $mm^2$/ cell confluency]. The area under the curve (AUC) values were calculated by
174 summing the proliferation or normalized dead cell number at each time point.

175

176 **Western blotting**

177 Cells were lysed in ice-cold RIPA buffer with protease inhibitors (Fisher Scientific, PIA32955) followed by
178 sonication in a water bath sonicator (Diagenode). Protein was quantified using the DC protein assay (Bio-
179 Rad). Lysates were prepared with 6X SDS sample buffer containing 12% (v/v) β-ME (VWR) and
180 separated on Bolt™ or NuPAGE 4-12% Bis-Tris gels (Invitrogen). SDS-PAGE separation was followed by
181 transfer to 0.45 µm nitrocellulose membranes (GE Healthcare). The membranes were blocked in 5% non-
182 fat milk in Tris-buffered saline with 0.1% Tween 20 (TBST). For immunoblotting, the following antibodies

183 diluted in 5% milk in TBST were used: KEAP1 (Millipore Sigma, RRID:AB_2921362, 1:2000), NRF2 (Cell
184 Signaling Technologies, D1Z9C, RRID:AB_2715528, 1:1000), NQO1 (Sigma Aldrich, RRID:AB_1079501,
185 1:1000), GCLC (Sana Cruz Biotechnology, H-5, RRID:AB_2736837, 1:1000), xCT (abcam,
186 RRID:AB_778944, 1:1000), GSR (Santa Cruz Biotechnology, RRID:AB_2295121, 1:1000), β-actin
187 (Invitrogen AM4302, RRID:AB_2536382, 1:100,000). HRP secondary antibodies used include goat anti-
188 rabbit IgG (Jackson ImmunoResearch Labs, RRID: AB_2313567), goat anti-mouse IgG (Jackson
189 ImmunoResearch Labs, RRID:AB_10015289), and goat anti-rat IgG (Jackson ImmunoResearch Labs,
190 RRID:AB_2338128). Membranes were developed with Clarity ECL substrate (Bio-Rad) or a luminol-
191 based homemade ECL substrate.

192

193 **Soft agar colony formation assays**

194 6-well plates were coated with a 0.8% agar prepared in RPMI. NSCLC cells were then seeded in 0.4%
195 agar in RPMI. After the cell/ agar mixture solidified, RPMI medium containing 10% FBS, Pen/Strep and
196 puromycin was added to each well and replenished every few days. Colonies were allowed to form for
197 10–16 days, and wells were stained with 0.01% crystal violet in a 4% paraformaldehyde in PBS solution.
198 Plates were scanned on a flatbed scanner and ImageJ was used to quantify colonies.

199

200 **DepMap Analysis**

201 *NFE2L2* dependency scores were downloaded from the DepMap database v. 22Q2 (45). Values were
202 plotted from CRISPR (DepMap 22Q2 Public+Score, Chronos) for non-small cell lung cancer cell lines that
203 we previously evaluated for high or low NRF2 activity (24).

204

205 **Quantification and statistical analysis**

206 Graphpad Prism9 software was used for statistical analyses and P values < 0.05 were considered
207 significant, with symbols as follows: *p<0.05, **p<0.01, ***p<0.001, ****p<0.0001. All data is represented

208 as mean +/- standard deviation unless otherwise stated. For all experiments, similar variances between
209 groups were observed.

210

211 **Data Availability**

212 The data generated in this study are included in the article and its supplementary figures. Raw data are
213 available upon request without restriction from the corresponding author. The gene expression data
214 generated in this study are publicly available in Gene Expression Omnibus (GEO) at GSE212942.

215

## 216 Results

### 217 *Keap1*$^{R554Q}$ and *Nfe2l2*$^{D29H}$ alleles activate the Nrf2 transcriptional program

218 To study the role of NRF2 activation in lung cancer, we developed alleles harboring either the Keap1$^{R554Q}$
219 or the Nrf2$^{D29H}$ mutation found in human NSCLC **(Fig. 1A** and **B)**. Both Keap1$^{R554Q}$ and Nrf2$^{D29H}$ mutations
220 prevent Keap1-mediated ubiquitination of Nrf2, allowing for constitutive expression of Nrf2 and
221 transcription of Nrf2 target genes (46, 47). To generate the conditionally active *(CA)-Keap1*$^{R554Q}$ allele, we
222 inserted a wild-type *Keap1* cDNA containing exons 3-5 flanked by loxP sites upstream of the R554Q
223 mutation in endogenous exon 4 of the *Keap1* gene **(Fig. 1A)** (32). For the Lox-STOP-Lox *(LSL)-*
224 *Nfe2l2*$^{D29H}$ allele, we inserted a loxP-flanked transcriptional and translational STOP (LSL) cassette
225 upstream of the D29H mutation in exon 2 of the endogenous *Nfe2l2* gene **(Fig. 1B).** For both alleles, Cre-
226 mediated excision of loxP-flanked cassettes allows for physiological expression of Keap1$^{R554Q}$ or Nrf2$^{D29H}$,
227 recapitulating NRF2 activation in human NSCLC. To validate the functionality of these alleles, we first
228 generated mouse embryonic fibroblasts (MEFs), which allowed the switching from a Nrf2 deficient state
229 (Nrf2$^{LSL/LSL}$) to a Nrf2 stabilized state (Nrf2$^{D29H/D29H}$), or from a basal Nrf2 state (Keap1$^{+/+}$) to a stabilized
230 Nrf2 state (Keap1$^{R554Q/R554Q}$) in an isogenic system. Using these MEFs, we performed both transcriptomic
231 profiling **(Fig. 1C** and **D)**. RNA-sequencing indicated that both Keap1$^{R554Q/R554Q}$ and Nrf2$^{D29H/D29H}$ MEFs
232 demonstrated increased transcription of canonical Nrf2 target genes, including Nqo1, Srxn1, Txnrd1, and
233 Gclc **(Fig. 1C** and **D)**. Prior targeting of the murine *Keap1* locus to generate a *Keap1*$^{flox}$ allele resulted in

234 the generation of a hypomorphic allele prior to Cre-mediated recombination, leading to decreased Keap1
235 levels and increased Nrf2 transcriptional activity throughout the whole animal (48). Importantly, we found
236 no differences in expression of Keap1, Nrf2, or Nrf2 target proteins Nqo1 and Gclc between CA-
237 Keap1$^{R554Q}$ and WT Keap1 MEFs, indicating that the *CA-Keap1*$^{R554Q}$ allele is not hypomorphic
238 (Supplementary Fig. S1). Collectively, these results indicate that the mutant *Keap1*$^{R554Q}$ and *Nfe2l2*$^{D29H}$
239 alleles activate the Nrf2 transcriptional program.

240

241 **Keap1 or Nrf2 mutation is not sufficient to initiate lung tumorigenesis**

242 Given the importance of NRF2 in cytoprotection and redox homeostasis, there has been a longstanding
243 interest in activating NRF2 pharmacologically for chemoprevention(8-10). The long-term safety of this
244 approach, and whether the chronic activation of NRF2 can transform healthy cells *in vivo*, remains
245 unknown. Moreover, the whole body deletion of Keap1 in mice results in postnatal lethality because of
246 constitutive Nrf2 activation (49). In human lung tumors, *KEAP1* inactivation is frequently biallelic(13),
247 whereas *NFE2L2* mutations are frequently heterozygous (50). Therefore, we induced the recombination
248 of *Keap1* and *Nfe2l2* alleles in the lungs of Keap1$^{R554Q/+}$, Keap1$^{R554Q/R554Q}$, or Nrf2$^{D29H/+}$ mice using
249 adenoviral-Cre to test whether constitutive Nrf2 activation is sufficient to initiate lung tumor formation **(Fig.**
250 **2)**. First, we analyzed the overall survival between the different groups. The median survival across
251 genotypes ranged from approximately 650-750 days, with no significant survival differences observed
252 between wild-type and Keap1/Nrf2 mutant groups **(Fig. 2A)**. While mice did develop tumors, they
253 comprised age-associated tumors like lymphoma. Upon examination of mouse lung histology for the
254 presence of lung tumors, lung tumor-free survival was also not different between the groups **(Fig. 2B)**.
255 Finally, histological analysis of lung tissues revealed that both alveolar and bronchiolar cells appeared
256 phenotypically normal across the genotypes **(Fig. 2C)**. These results indicate that constitutive Nrf2
257 activation is not sufficient to induce lung tumor formation.

258

259 **Keap1 or Nrf2 mutation is not sufficient to initiate lung tumorigenesis in combination with tumor**
260 **suppressor loss**

261 To determine whether tumor suppressor loss was required for mutant Keap1 or Nrf2 to initiate lung tumor
262 formation, we crossed Keap1 and Nrf2 mutant mice with p53$^{flox}$ and Lkb1$^{flox}$ alleles to concomitantly
263 activate Nrf2 and delete these tumor suppressors in the lung **(Fig. 3)**. We first examined the consequence
264 of Nrf2$^{D29H/+}$, Keap1$^{R554Q/+}$, or Keap1$^{R554Q/R554Q}$ in combination with p53 deletion. Mice were aged to 500
265 days, at which time all mice were euthanized and examined for evidence of lung tumor formation. While a
266 small number of these mice did succumb to disease prior to 500 days, they developed age-associated
267 tumors including lymphoma, and we did not observe any differences in overall or lung tumor-free survival
268 between genotypes **(Fig. 3A** and **B)**. However, when examining the lung tissue histology, we observed
269 dysplasia in Keap1$^{R554Q/R554Q}$ bronchioles following loss of p53 **(Fig. 3C)**. This observation is consistent
270 with previous work showing that tracheospheres derived from *Keap1*$^{-/-}$;*Trp53*$^{-/-}$ cells had an aberrant
271 morphology (31). We next examined the consequence of Nrf2$^{D29H/+}$, Keap1$^{R554Q/+}$ or Keap1$^{R554Q/R554Q}$ in
272 combination with Lkb1 deletion. Similar to what was observed with p53, we also did not find any
273 differences in overall or lung tumor-free survival between cohorts **(Fig. 3D** and **E)**. Moreover, the
274 bronchiolar and alveolar morphology was normal across genotypes, in contrast to what was observed
275 upon p53 loss **(Fig. 3F)**. Our findings indicate that Keap1/Nrf2 mutation is not sufficient to initiate lung
276 tumor formation in combination with tumor suppressor loss.

277

278 **Nrf2 activation cooperates with mutant Kras to promote lung tumor initiation and early**
279 **progression**

280 We and others have reported that Nrf2 activation is important for Kras mutant lung tumorigenesis (23, 29,
281 30). To understand how Keap1 or Nrf2 mutation affect lung tumor initiation and early progression, we
282 crossed Keap1/Nrf2 mutant mice with the Kras$^{G12D/+}$ model of early lung adenocarcinoma (40). While all
283 mice succumbed to lung tumors with a median survival of around 200 days, we observed no difference in
284 survival between cohorts **(Fig. 4A** and **B)**. We next validated that these mutations were activating toward
285 Nrf2 in tumors by performing immunohistochemical staining for Nrf2 and the Nrf2 target Nqo1. We
286 observed that Keap1$^{R554Q/R554Q}$ expression resulted in the greatest degree of Nrf2 activation, followed by
287 Nrf2$^{D29H/+}$, and then Keap1$^{R554Q/+}$ compared to Keap1/Nrf2$^{+/+}$ expression **(Fig. 4C-F)**. To examine the

288 influence of Nrf2 activation on tumor initiation, we quantified tumor number across the genotypes and
289 found that Keap1$^{R554Q/R554Q}$ and Nrf2$^{D29H/+}$ significantly increased tumor number in the Kras$^{G12D/+}$ model
290 **(Fig. 4G** and **H)**, consistent with prior reports using Keap1 deletion models (29, 30). We then examined
291 the influence of Nrf2 on tumor progression by analyzing tumor grade. The distribution of atypical
292 adenomatous and bronchiolar hyperplasia (AAH and BH, respectively) and tumors from grades 1
293 (adenoma) to 5 (adenocarcinoma) was determined. We observed an increase in the proportion and
294 number of grade 1 tumors in Keap1$^{R554Q/R554Q}$ and Nrf2$^{D29H/+}$ mice compared to Keap1$^{R554Q/+}$ and
295 Keap1/Nrf2$^{+/+}$ mice **(Fig. 4I,** Supplementary Fig. S2A). We also examined tumor size by grade and found
296 that the median tumor size did not differ across genotypes (Supplementary Fig. S2B), although there
297 were some modest differences across the individual grades, including decreased AAH size in all
298 Keap1/Nrf2 mutant models (Supplementary Fig. S2C). Moreover, we found that there was a decrease in
299 grade 3 tumor burden across all Keap1 and Nrf2 mutant models **(Fig. 4J)**, which resulted in a decreased
300 overall tumor burden (Supplementary Fig. S2D) because grade 3 tumors were much larger than other
301 grades (Supplementary Fig. S2C). Grade 3 tumors were extremely rare in the Kras$^{G12D/+}$ model, however,
302 limiting our ability to draw conclusions on the influence of Nrf2 activation on a limited number of tumors.
303 Our findings indicate that Kras$^{G12D/+}$ mutation cooperates with Keap1/Nrf2 mutation to promote formation
304 of lung tumors and early progression to low-grade tumors.

305

306 **Nrf2 activation impairs lung adenocarcinoma progression**

307 The decrease in grade 3 tumor burden in the Keap1/Nrf2 mutant models suggested that Nrf2 activation
308 may impair progression to higher grade tumors. We next used the Kras$^{G12D/+}$; p53$^{fl/fl}$ (KP) model, which
309 develops advanced-grade lung adenocarcinomas (43). We previously reported that the expression of
310 Keap1$^{R554Q/R554Q}$ dramatically decreased overall tumor size in this model (32), but other groups have
311 found differing effects of Nrf2 activation. While some studies reported that Keap1 inactivation promoted
312 adenocarcinoma progression (33, 34), others reported that Keap1 deletion did not affect tumor size(36,
313 37), but the conditions used and phenotypes assayed varied across these studies. Thus, we decided to
314 perform comprehensive phenotyping on KP tumors following Nrf2 activation. Similar to what we observed

315 in the Kras$^{G12D/+}$ model, we found that overall survival of the KP model was not affected by Keap1 or Nrf2
316 mutation **(Fig. 5A** and **B)**. Moreover, we found that Keap1/Nrf2 mutation affected Nrf2 activation in a
317 similar manner to the Kras$^{G12D/+}$ model, with Keap1$^{R554Q/R554Q}$ being the most activating, followed by
318 Nrf2$^{D29H/+}$, and then Keap1$^{R554Q/+}$ compared to Keap1/Nrf2$^{+/+}$ mice **(Fig. 5C-F)**. From the histology images,
319 it was very apparent that Keap1$^{R554Q/R554Q}$ mice had decreased overall tumor burden **(Fig. 5G)**, which was
320 confirmed upon quantitation (Supplementary Fig. S3A). Next, we examined tumor progression by tumor
321 grading and found a significant decrease in the proportion, number, and burden of grade 3 and 4 tumors
322 in the Keap1$^{R554Q/R554Q}$ cohort **(Fig. 5G** and **H,** Supplementary Fig. S3B). We also observed a modest,
323 non-significant decrease in the proportion, number, and burden of grade 3 and 4 tumors in the Nrf2$^{D29H/+}$
324 cohort **(Fig. 5G** and **H**, Supplementary Fig. S3B), further supporting a threshold for Nrf2 to impair tumor
325 progression. Additionally, we saw an increase in the proportion, number, and burden of grade 1 tumors in
326 the Keap1$^{R554Q/R554Q}$ group, suggesting that there may be a threshold for Nrf2 activation to promote early
327 progression, but impair late progression **(Fig. 5G** and **H,** Supplementary Fig. S3B). While there were no
328 differences in overall median tumor size (Supplementary Fig. S3C), Keap1$^{R554Q/R554Q}$ alveolar hyperplasia
329 and grade 1 tumors were significantly smaller compared to their wild-type counterparts (Supplementary
330 Fig. S3D). Consistently, we found a decrease in tumor cell proliferation in the Keap1$^{R554Q/R554Q}$ cohort,
331 specifically in AAH and grade 1/2 tumors, and no tumor cell death was observed (Supplementary Fig.
332 S3E-H). Importantly, despite the reduction in grade 1 size, the higher grade 1 burden in Keap1$^{R554Q/R554Q}$
333 mice was accounted for by the increase in the total number of grade 1 tumors (Supplementary Fig. S3B
334 and I), highlighting that burden is a complex measurement influenced by multiple variables. We next
335 investigated whether tumors that progressed to the adenocarcinoma stage altered Nrf2 expression and/or
336 activity. To this end, we analyzed Nrf2 and Nqo1 levels across all tumor grades and hyperplasia (AAH,
337 BH). We found that Nrf2 and Nqo1 levels were highly elevated in Keap1/Nrf2 mutant grade 1 tumors, with
338 Nqo1 demonstrating increased nuclear localization in homozygous Keap1 mutant tumors compared to
339 Nrf2 mutant tumors **(Fig. 6A)**. However, as tumors progressed to higher grades, Nrf2 and Nqo1
340 expression were reduced in the Keap1/Nrf2 mutant models **(Fig. 6A-C)**. These results suggest that Nrf2
341 activation beyond a certain threshold impairs advanced-grade tumor progression, requiring selection for a
342 more tolerable level of Nrf2 expression and activity in high-grade tumors.

343

344 **NRF2 overexpression impairs NSCLC cell proliferation, viability, and anchorage-independent**
345 **colony formation**

346 KEAP1 has other substrates (51-56), raising the question of whether NRF2 plays a causal role in tumor
347 suppression. It was previously reported that KEAP1 mutant lung cancer cell lines are "NRF2 addicted"
348 and dependent on NRF2 for proliferation (57). Supportingly, analysis of DepMap data (45) revealed that
349 NSCLC cell lines with high NRF2 activity (24), which were enriched for KEAP1 mutations, exhibited NRF2
350 dependence **(Fig. 7A)**. To directly test the hypothesis that excessive NRF2 activation above a specific
351 threshold is detrimental to lung tumor cell growth, we used lentiviral transduction to overexpress NRF2 in
352 five KEAP1 mutant lung cancer cell lines (H1944, H322, A549, HCC15, H460). We confirmed
353 overexpression of NRF2 by western blot analysis of NRF2 and target genes GCLC, xCT, and GSR **(Fig.**
354 **7B)**. Lentiviral transduction increased the expression of NRF2 in all cell lines, and increased the
355 expression of NRF2 targets, demonstrating that NRF2 binding sites were not saturated by the level of
356 NRF2 in these cell lines **(Fig. 7B)**. Next, we determined the influence of NRF2 overexpression on cellular
357 proliferation and death over the course of four days using live cell imaging **(Fig. 7C-G)**. Like what we
358 observed in the $Kras^{G12D/+}$; $p53^{fl/fl}$ model upon $Keap1^{R554Q/R554Q}$ expression, we found that NRF2
359 overexpression decreased cell proliferation in all cell lines **(Fig. 7F)**. Moreover, Nrf2 overexpression
360 increased cell death in 4 out of 5 cell lines **(Fig. 7G)**. Finally, we observed impaired anchorage-
361 independent growth in soft agar in all cell lines **(Fig. 7H** and **I)**. These results indicate that there is an
362 optimal threshold of NRF2 activity, and that excess NRF2 activation can impair lung cancer phenotypes.

363

364 **Single copy Nrf2 deletion rescues homozygous $Keap1^{R554Q}$-mediated tumor progression**
365 **impairment**

366 To directly examine whether reducing Nrf2 levels could alleviate the block in adenocarcinoma progression
367 in the $Keap1^{R554Q/R554Q}$ model, we crossed a $Nrf2^{flox}$ allele into both our $Kras^{G12D/+}$; $p53^{fl/fl}$ and $Kras^{G12D/+}$;
368 $p53^{fl/fl}$; $Keap1^{R554Q/R554Q}$ models. Because we previously found that complete Nrf2 deficiency impairs
369 tumor initiation (23), we examined the consequence of single copy Nrf2 deletion on tumor phenotypes.

370 Again, we found no difference in overall survival between groups **(Fig. 8A)**. We also observed that Nrf2
371 deletion in the Keap1$^{R554Q/R554Q}$ model significantly decreased expression of Nrf2 and Nqo1 **(Fig. 8B-E,**
372 Supplementary Fig. S4). Moreover, histological examination of the lungs revealed a striking difference in
373 tumor burden, with Nrf2 heterozygous deletion having a minimal effect on the Kras$^{G12D/+}$; p53$^{fl/fl}$ model
374 while dramatically increasing burden in the Kras$^{G12D/+}$; p53$^{fl/fl}$; Keap1$^{R554Q/R554Q}$ model **(Fig. 8F,**
375 Supplementary Fig. S5A). Tumor size was not affected (Supplementary Fig. S5B and C). Next, we
376 examined tumor progression in these models. In agreement with our previous experiment **(Fig. 5H)**, we
377 found that the Keap1$^{R554Q/R554Q}$ cohort had a significant reduction in adenocarcinoma progression upon
378 Nrf2$^{WT}$ expression **(Fig. 8G)**. However, upon single copy Nrf2 deletion (Nrf2$^{flox/+}$), Keap1$^{R554Q/R554Q}$ failed to
379 suppress tumor progression **(Fig. 8G)**. Moreover, the decrease in grade 3 tumor number and burden
380 induced by Keap1$^{R554Q/R554Q}$ was alleviated by single copy deletion of Nrf2 **(Fig. 8H,** Supplementary Fig.
381 **S5D** and **E)**. These results demonstrate that there is a threshold by which Nrf2 activation can promote or
382 impair tumor initiation or progression.

383

384 ## Discussion

385 Using genetically engineered mouse models of Keap1/Nrf2 mutation, we find that Keap1 or Nrf2
386 mutations alone are insufficient to cause lung tumor formation. Even in combination with tumor
387 suppressor loss, we did not observe lung tumor formation after 500 days, suggesting that chronic NRF2
388 activation would be a safe strategy for chemoprevention. These findings corroborate previous studies
389 showing that Keap1 deletion does not induce lung tumor development (28), even in the absence of tumor
390 suppressors p53 or Lkb1 (29), out to 12-15 months. In combination with Kras$^{G12D/+}$ mutation, we found
391 that Nrf2 activation promoted tumor initiation. Our results are consistent with previous work indicating that
392 Nrf2 activation via Keap1 deletion promotes Kras$^{G12D/+}$ tumor initiation (29, 30). Surprisingly, we find that
393 Nrf2 activation impairs tumor progression, which is correlated with Nrf2 dosage. In our previous study with
394 Keap1$^{R554Q/R554Q}$ mice, we reported smaller tumors in the KP model (32), which we now find is due to
395 impaired tumor progression mediated by Nrf2 hyperactivation. Because most prior studies from other
396 groups did not specifically analyze tumor grade (27, 29, 36, 37), they may not have captured this effect of

397 Nrf2 on tumor progression. Alternatively, there may be biological differences between Keap1 deletion and
398 mutation. Moreover, the dosage-dependent effects of Nrf2 that we found are also reminiscent of what has
399 been observed for oncogenes like Ras and Myc, where low levels promote transformation and
400 proliferation, and high levels promote senescence or death (58, 59).

401

402 Our findings that tumors downregulate Nrf2 to select for a level permissive for tumor progression and that
403 ectopic NRF2 expression antagonizes the proliferation and viability of human NSCLC cells are supported
404 by our finding that single copy deletion of Nrf2 can rescue the homozygous Keap1$^{R554Q}$-mediated block in
405 tumor progression. This result demonstrates a direct role for Nrf2 hyperactivation but we cannot exclude
406 the possibility that alternative KEAP1 substrates, such as PGAM5 (51), PALB2 (52), MCM3 (53) or EMSY
407 (54), contribute to the block in tumor progression. In agreement with our findings, a Keap1-binding
408 defective Nrf2$^{E79Q}$ mouse model of small-cell lung cancer (SCLC) with p53/ p16 inactivation (60) also
409 displayed Nrf2 downregulation in aggressive SCLC tumors. The exact mechanism(s) by which high NRF2
410 activity impairs tumor cell proliferation and tumor progression remains to be determined. NRF2 activation
411 is associated with multiple metabolic liabilities that could explain this phenotype, including CDO1-
412 mediated toxic metabolite formation and NADPH depletion (32), xCT-mediated glutamate depletion (26,
413 34, 61), and ALDH3A1-mediated reductive stress (62). Future studies are needed to determine if these or
414 other mechanisms play a role in NRF2-mediated proliferation and progression impairment.

415

416 Given that KEAP1 and NRF2 mutations are found with a high frequency in human NSCLC and are
417 associated with poor outcomes, these findings raise the question of under which contexts NRF2
418 activation provides an advantage. Our findings that NRF2/KEAP1 mutation promotes tumor initiation are
419 consistent with recent results from the TRACERx study, where *KEAP1* mutations were found to be an
420 initiating driver together with *KRAS* and *TP53* mutations in lung adenocarcinoma (63), and suggest that
421 additional genetic events may be needed to overcome NRF2-mediated inhibition of tumor progression.
422 We did not find that these mutations conferred poor outcomes in our mouse models, but there are
423 multiple features of patient tumors not captured by our models that remain to be examined. They did not

424 develop metastases with sufficient frequency, precluding an examination of the influence of Nrf2
425 activation on metastasis as reported previously (27). Moreover, mice are not exposed to smoking and
426 other environmental toxins under which NRF2 activation may promote survival (4-7). We have also not
427 tested the response of these models to therapy. Additional mechanistic studies are warranted to clarify
428 the clinical translation of these approaches, including understanding how NRF2 is downregulated upon
429 progression and the consequences of NRF2 pharmacological activation and inhibition on the various
430 tumor grades in our GEMM models. These studies will be important to compare the level of NRF2
431 achieved with pharmacological manipulation to the level induced by KEAP1/NRF2 mutation and where
432 that falls on the threshold spectrum. Moreover, our models are designed to only activate NRF2 in cancer
433 cells while these pharmacological agents will modulate NRF2 in the microenvironment, which will also
434 influence tumor growth (30, 64, 65). These future studies will further clarify the context-dependent role of
435 NRF2 during the complex stages of tumorigenesis.

436

437 **Acknowledgements**

438 This work was supported by grants from the NIH/NCI (R37-CA230042), the American Lung Association
439 (LCDA-498544) and the American Cancer Society's Institutional Research Grant to G.M.D. This work was
440 also supported by the Analytical Microscopy and the Tissue Core Facilities at the Moffitt Cancer Center,
441 an NCI designated Comprehensive Cancer Center (P30-CA076292). We would like to thank the DeNicola
442 lab members and Dr. Ana Gomes for the helpful discussions. We thank Cheyenne Schneider for
443 proofreading.

444

445

446

447 **References**


448 1. DeBlasi JM, DeNicola GM. Dissecting the Crosstalk between NRF2 Signaling and
449 Metabolic Processes in Cancer. Cancers (Basel). 2020;12(10).
450 2. He F, Ru X, Wen T. NRF2, a Transcription Factor for Stress Response and Beyond. Int J
451 Mol Sci. 2020;21(13).
452 3. Itoh K, Wakabayashi N, Katoh Y, Ishii T, Igarashi K, Engel JD, et al. Keap1 represses
453 nuclear activation of antioxidant responsive elements by Nrf2 through binding to the amino-
454 terminal Neh2 domain. Genes Dev. 1999;13(1):76-86.
455 4. Ramos-Gomez M, Dolan PM, Itoh K, Yamamoto M, Kensler TW. Interactive effects of
456 nrf2 genotype and oltipraz on benzo[ a ]pyrene–DNA adducts and tumor yield in mice.
457 Carcinogenesis. 2003;24(3):461-7.
458 5. Ramos-Gomez M, Kwak M-K, Dolan PM, Itoh K, Yamamoto M, Talalay P, et al. Sensitivity
459 to carcinogenesis is increased and chemoprotective efficacy of enzyme inducers is lost in
460 nrf2 transcription factor-deficient mice. Proceedings of the National Academy of
461 Sciences. 2001;98(6):3410-5.
462 6. Aoki Y, Sato H, Nishimura N, Takahashi S, Itoh K, Yamamoto M. Accelerated DNA adduct
463 formation in the lung of the Nrf2 knockout mouse exposed to diesel exhaust. Toxicol Appl
464 Pharmacol. 2001;173(3):154-60.
465 7. Iida K, Itoh K, Kumagai Y, Oyasu R, Hattori K, Kawai K, et al. Nrf2 Is Essential for the
466 Chemopreventive Efficacy of Oltipraz against Urinary Bladder Carcinogenesis. Cancer Research.
467 2004;64(18):6424-31.
468 8. Kensler TW, Wakabayashi N. Nrf2: friend or foe for chemoprevention? Carcinogenesis.
469 2010;31(1):90-9.
470 9. Schmidlin CJ, Shakya A, Dodson M, Chapman E, Zhang DD. The intricacies of NRF2
471 regulation in cancer. Semin Cancer Biol. 2021;76:110-9.
472 10. Telkoparan-Akillilar P, Suzen S, Saso L. Pharmacological Applications of Nrf2 Inhibitors as
473 Potential Antineoplastic Drugs. Int J Mol Sci. 2019;20(8).
474 11. Network CGAR. Comprehensive molecular profiling of lung adenocarcinoma. Nature.
475 2014;511(7511):543-50.
476 12. Network CGAR. Comprehensive genomic characterization of squamous cell lung cancers.
477 Nature. 2012;489(7417):519-25.
478 13. Singh A, Misra V, Thimmulappa RK, Lee H, Ames S, Hoque MO, et al. Dysfunctional
479 KEAP1-NRF2 interaction in non-small-cell lung cancer. PLoS Med. 2006;3(10):e420.
480 14. Shibata T, Ohta T, Tong KI, Kokubu A, Odogawa R, Tsuta K, et al. Cancer related
481 mutations in NRF2 impair its recognition by Keap1-Cul3 E3 ligase and promote malignancy. Proc
482 Natl Acad Sci U S A. 2008;105(36):13568-73.
483 15. Wang R, An J, Ji F, Jiao H, Sun H, Zhou D. Hypermethylation of the Keap1 gene in human
484 lung cancer cell lines and lung cancer tissues. Biochem Biophys Res Commun. 2008;373(1):151-
485 4.
486 16. Kim YR, Oh JE, Kim MS, Kang MR, Park SW, Han JY, et al. Oncogenic NRF2 mutations in
487 squamous cell carcinomas of oesophagus and skin. J Pathol. 2010;220(4):446-51.
488 17. Zhang P, Singh A, Yegnasubramanian S, Esopi D, Kombairaju P, Bodas M, et al. Loss of
489 Kelch-like ECH-associated protein 1 function in prostate cancer cells causes chemoresistance
490 and radioresistance and promotes tumor growth. Mol Cancer Ther. 2010;9(2):336-46.

491 18. Solis LM, Behrens C, Dong W, Suraokar M, Ozburn NC, Moran CA, et al. Nrf2 and Keap1
492 abnormalities in non-small cell lung carcinoma and association with clinicopathologic features.
493 Clin Cancer Res. 2010;16(14):3743-53.
494 19. Wang Q, Xu L, Wang G, Chen L, Li C, Jiang X, et al. Prognostic and clinicopathological
495 significance of NRF2 expression in non-small cell lung cancer: A meta-analysis. PLoS One.
496 2020;15(11):e0241241.
497 20. Zhao J, Lin X, Meng D, Zeng L, Zhuang R, Huang S, et al. Nrf2 Mediates Metabolic
498 Reprogramming in Non-Small Cell Lung Cancer. Front Oncol. 2020;10:578315.
499 21. Sporn MB, Liby KT. NRF2 and cancer: the good, the bad and the importance of context.
500 Nat Rev Cancer. 2012;12(8):564-71.
501 22. Singh A, Bodas M, Wakabayashi N, Bunz F, Biswal S. Gain of Nrf2 function in non-small-
502 cell lung cancer cells confers radioresistance. Antioxidants and Redox Signaling. 2010.
503 23. Denicola GM, Karreth FA, Humpton TJ, Gopinathan A, Wei C, Frese K, et al. Oncogene-
504 induced Nrf2 transcription promotes ROS detoxification and tumorigenesis. Nature.
505 2011;475(7354):106-10.
506 24. DeNicola GM, Chen PH, Mullarky E, Sudderth JA, Hu Z, Wu D, et al. NRF2 regulates
507 serine biosynthesis in non-small cell lung cancer. Nature Genetics. 2015;47(12):1475-81.
508 25. Mitsuishi Y, Taguchi K, Kawatani Y, Shibata T, Nukiwa T, Aburatani H, et al. Nrf2 redirects
509 glucose and glutamine into anabolic pathways in metabolic reprogramming. Cancer Cell.
510 2012;22(1):66-79.
511 26. Sayin VI, LeBoeuf SE, Singh SX, Davidson SM, Biancur D, Guzelhan BS, et al. Activation of
512 the NRF2 antioxidant program generates an imbalance in central carbon metabolism in cancer.
513 Elife. 2017;6.
514 27. Lignitto L, LeBoeuf SE, Homer H, Jiang S, Askenazi M, Karakousi TR, et al. Nrf2 Activation
515 Promotes Lung Cancer Metastasis by Inhibiting the Degradation of Bach1. Cell.
516 2019;178(2):316-29.e18.
517 28. Best SA, De Souza DP, Kersbergen A, Policheni AN, Dayalan S, Tull D, et al. Synergy
518 between the KEAP1/NRF2 and PI3K Pathways Drives Non-Small-Cell Lung Cancer with an
519 Altered Immune Microenvironment. Cell Metabolism. 2018;27(4):935-43.e4.
520 29. Best SA, Ding S, Kersbergen A, Dong X, Song JY, Xie Y, et al. Distinct initiating events
521 underpin the immune and metabolic heterogeneity of KRAS-mutant lung adenocarcinoma.
522 Nature Communications. 2019;10(1):1-14.
523 30. Hayashi M, Kuga A, Suzuki M, Panda H, Kitamura H, Motohashi H, et al.
524 Microenvironmental Activation of Nrf2 Restricts the Progression of Nrf2-Activated Malignant
525 Tumors. Cancer Res. 2020;80(16):3331-44.
526 31. Jeong Y, Hoang NT, Lovejoy A, Stehr H, Newman AM, Gentles AJ, et al. Role of
527 KEAP1/NRF2 and TP53 mutations in lung squamous cell carcinoma development and radiation
528 resistance. Cancer Discovery. 2017;7(1):86-101.
529 32. Kang YP, Torrente L, Falzone A, Elkins CM, Liu M, Asara JM, et al. Cysteine dioxygenase 1
530 is a metabolic liability for non-small cell lung cancer. eLife. 2019.
531 33. Romero R, Sánchez-Rivera FJ, Westcott PMK, Mercer KL, Bhutkar A, Muir A, et al. Keap1
532 mutation renders lung adenocarcinomas dependent on Slc33a1. Nature Cancer. 2020;1(6):589-
533 602.

534 34. Romero R, Sayin VI, Davidson SM, Bauer MR, Singh SX, Leboeuf SE, et al. Keap1 loss
535 promotes Kras-driven lung cancer and results in dependence on glutaminolysis. Nature
536 Medicine. 2017.
537 35. Singh A, Daemen A, Nickles D, Jeon S-M, Foreman O, Sudini K, et al. NRF2 Activation
538 Promotes Aggressive Lung Cancer and Associates with Poor Clinical Outcomes. Clinical Cancer
539 Research. 2021;27(3):877.
540 36. Foggetti G, Li C, Cai H, Hellyer JA, Lin W-Y, Ayeni D, et al. Genetic Determinants of EGFR-
541 Driven Lung Cancer Growth and Therapeutic Response In Vivo. Cancer Discovery.
542 2021;11(7):1736-53.
543 37. Rogers ZN, McFarland CD, Winters IP, Seoane JA, Brady JJ, Yoon S, et al. Mapping the in
544 vivo fitness landscape of lung adenocarcinoma tumor suppression in mice. Nature Genetics.
545 2018.
546 38. Cai H, Chew SK, Li C, Tsai MK, Andrejka L, Murray CW, et al. A Functional Taxonomy of
547 Tumor Suppression in Oncogenic KRAS-Driven Lung Cancer. Cancer Discov. 2021;11(7):1754-73.
548 39. Rogers ZN, McFarland CD, Winters IP, Naranjo S, Chuang C-H, Petrov D, et al. A
549 quantitative and multiplexed approach to uncover the fitness landscape of tumor suppression
550 in vivo. Nature Methods. 2017;14(7):737-42.
551 40. Jackson EL, Willis N, Mercer K, Bronson RT, Crowley D, Montoya R, et al. Analysis of lung
552 tumor initiation and progression using conditional expression of oncogenic K-ras. Genes and
553 Development. 2001.
554 41. McLoughlin MR, Orlicky DJ, Prigge JR, Krishna P, Talago EA, Cavigli IR, et al. TrxR1, Gsr,
555 and oxidative stress determine hepatocellular carcinoma malignancy. Proc Natl Acad Sci U S A.
556 2019;116(23):11408-17.
557 42. Bankhead P, Loughrey MB, Fernandez JA, Dombrowski Y, McArt DG, Dunne PD, et al.
558 QuPath: Open source software for digital pathology image analysis. Sci Rep. 2017;7(1):16878.
559 43. Jackson EL, Olive KP, Tuveson DA, Bronson R, Crowley D, Brown M, et al. The differential
560 effects of mutant p53 alleles on advanced murine lung cancer. Cancer Research.
561 2005;65(22):10280-8.
562 44. Berger AH, Brooks AN, Wu X, Shrestha Y, Chouinard C, Piccioni F, et al. High-throughput
563 Phenotyping of Lung Cancer Somatic Mutations. Cancer Cell. 2016;30(2):214-28.
564 45. Institute B. DepMap Public 22Q2 2022.
565 46. Hast BE, Cloer EW, Goldfarb D, Li H, Siesser PF, Yan F, et al. Cancer-derived mutations in
566 KEAP1 impair NRF2 degradation but not ubiquitination. Cancer Research. 2014.
567 47. Tong KI, Padmanabhan B, Kobayashi A, Shang C, Hirotsu Y, Yokoyama S, et al. Different
568 Electrostatic Potentials Define ETGE and DLG Motifs as Hinge and Latch in Oxidative Stress
569 Response. Molecular and Cellular Biology. 2007.
570 48. Taguchi K, Maher JM, Suzuki T, Kawatani Y, Motohashi H, Yamamoto M. Genetic
571 Analysis of Cytoprotective Functions Supported by Graded Expression of Keap1. Molecular and
572 Cellular Biology. 2010.
573 49. Wakabayashi N, Itoh K, Wakabayashi J, Motohashi H, Noda S, Takahashi S, et al. Keap1-
574 null mutation leads to postnatal lethality due to constitutive Nrf2 activation. Nature Genetics.
575 2003.

576 50. Huppke P, Weissbach S, Church JA, Schnur R, Krusen M, Dreha-Kulaczewski S, et al.
577 Activating de novo mutations in NFE2L2 encoding NRF2 cause a multisystem disorder. Nature
578 Communications. 2017;8(1):818.
579 51. Lo SC, Hannink M. PGAM5 tethers a ternary complex containing Keap1 and Nrf2 to
580 mitochondria. Exp Cell Res. 2008;314(8):1789-803.
581 52. Ma J, Cai H, Wu T, Sobhian B, Huo Y, Alcivar A, et al. PALB2 interacts with KEAP1 to
582 promote NRF2 nuclear accumulation and function. Mol Cell Biol. 2012;32(8):1506-17.
583 53. Mulvaney KM, Matson JP, Siesser PF, Tamir TY, Goldfarb D, Jacobs TM, et al.
584 Identification and characterization of MCM3 as a kelch-like ECH-associated protein 1 (KEAP1)
585 substrate. Journal of Biological Chemistry. 2016;291(45):23719-33.
586 54. Marzio A, Kurz E, Sahni JM, Di Feo G, Puccini J, Jiang S, et al. EMSY inhibits homologous
587 recombination repair and the interferon response, promoting lung cancer immune evasion.
588 Cell. 2022;185(1):169-83.e19.
589 55. Zhang Y, Shi Z, Zhou Y, Xiao Q, Wang H, Peng Y. Emerging Substrate Proteins of Kelch-
590 like ECH Associated Protein 1 (Keap1) and Potential Challenges for the Development of Small-
591 Molecule Inhibitors of the Keap1-Nuclear Factor Erythroid 2-Related Factor 2 (Nrf2) Protein–
592 Protein Interaction. Journal of Medicinal Chemistry. 2020;1.
593 56. McCutcheon DC, Lee G, Carlos A, Montgomery JE, Moellering RE. Photoproximity
594 Profiling of Protein-Protein Interactions in Cells. J Am Chem Soc. 2020;142(1):146-53.
595 57. Kitamura H, Motohashi H. NRF2 addiction in cancer cells. Cancer Sci. 2018;109(4):900-
596 11.
597 58. Tuveson DA, Shaw AT, Willis NA, Silver DP, Jackson EL, Chang S, et al. Endogenous
598 oncogenic K-ras(G12D) stimulates proliferation and widespread neoplastic and developmental
599 defects. Cancer Cell. 2004;5(4):375-87.
600 59. Murphy DJ, Junttila MR, Pouyet L, Karnezis A, Shchors K, Bui DA, et al. Distinct
601 thresholds govern Myc's biological output in vivo. Cancer Cell. 2008;14(6):447-57.
602 60. Hamad SH, Montgomery SA, Simon JM, Bowman BM, Spainhower KB, Murphy RM, et al.
603 TP53, CDKN2A/P16, and NFE2L2/NRF2 regulate the incidence of pure- and combined-small cell
604 lung cancer in mice. Oncogene. 2022;41(25):3423-32.
605 61. Muir A, Danai LV, Gui DY, Waingarten CY, Lewis CA, Vander Heiden MG. Environmental
606 cystine drives glutamine anaplerosis and sensitizes cancer cells to glutaminase inhibition. Elife.
607 2017;6.
608 62. Weiss-Sadan T, Ge M, Hayashi M, Gohar M, Yao C-H, de Groot A, et al. NRF2 activation
609 induces NADH-reductive stress, providing a metabolic vulnerability in lung cancer. Cell
610 Metabolism. 2023.
611 63. Jamal-Hanjani M, Wilson GA, McGranahan N, Birkbak NJ, Watkins TBK, Veeriah S, et al.
612 Tracking the Evolution of Non–Small-Cell Lung Cancer. New England Journal of Medicine.
613 2017;376(22):2109-21.
614 64. Satoh H, Moriguchi T, Saigusa D, Baird L, Yu L, Rokutan H, et al. NRF2 Intensifies Host
615 Defense Systems to Prevent Lung Carcinogenesis, but After Tumor Initiation Accelerates
616 Malignant Cell Growth. Cancer Res. 2016;76(10):3088-96.
617 65. Satoh H, Moriguchi T, Taguchi K, Takai J, Maher JM, Suzuki T, et al. Nrf2-deficiency
618 creates a responsive microenvironment for metastasis to the lung. Carcinogenesis.
619 2010;31(10):1833-43.

620 **Figure Legends**

621

622 **Figure 1.**

623 Development of mutant *Keap1* and *Nfe2l2* alleles found in human lung cancer. **A,** The conditionally active
624 (CA)-*Keap1*$^{R554Q}$ allele was generated by inserting a loxP-flanked, wild type (WT) *Keap1* cDNA containing
625 exons 3-5 into intron 2 and introducing the R554Q mutation into endogenous exon 4 of the *Keap1* gene.
626 Prior to intranasal installation of adenoviral-Cre recombinase Keap1 is wild type. Once the floxed cargo is
627 excised, mutant Keap1$^{R554Q}$ is expressed. PA = poly A signal. **B,** The Lox-STOP-Lox *(LSL)-Nfe2l2*$^{D29H}$
628 allele was created by inserting a STOP cassette flanked by loxP sites into intron 1 and introducing the
629 D29H mutation in endogenous exon 2 of the *Nfe2l2* gene. Following Cre-mediated excision of the STOP
630 cassette, mutant Nrf2$^{D29H}$ is expressed. **C,** Volcano plot of RNA-sequencing data from murine embryonic
631 fibroblasts (MEFs) expressing Keap1$^{R554Q/R554Q}$ compared to Keap1$^{+/+}$. N=3, representative of two
632 individual MEF lines. **D,** Volcano plot of RNA-sequencing data from MEFs expressing Nrf2$^{D29H/D29H}$
633 compared to Nrf2$^{LSL/LSL}$, which lack Nrf2 expression. N=3, representative of two individual MEF lines.

634 **Figure 2.**

635 Mutation of Keap1 or Nrf2 is not sufficient to initiate lung tumorigenesis. **A,** Overall survival of Keap1/Nrf2
636 mutant mice. Keap1/Nrf2$^{+/+}$ (n=17), Keap1$^{R554Q/+}$ (n=8); Keap1$^{R554Q/R554Q}$ (n=11); Nrf2$^{D29H/+}$ (n=15). Ns= not
637 significant (Log-rank (Mantel-Cox) test). **B,** Lung tumor-free survival of Keap1/Nrf2 mutant mice.
638 Keap1/Nrf2$^{+/+}$ (n=11), Keap1$^{R554Q/+}$ (n=4); Keap1$^{R554Q/R554Q}$ (n=8); Nrf2$^{D29H/+}$ (n=11). **C,** Representative
639 H&E of mouse lung depicting normal bronchiolar and alveolar cells (scale bars = 100μM (top panel), 20
640 μM (bottom panel)).

641 **Figure 3.**

642 Mutation of Keap1 or Nrf2 is not sufficient to initiate lung tumorigenesis with p53 or Lkb1 loss. **A,** Overall
643 survival of p53$^{fl/fl}$ mice expressing wild-type or mutant Keap1/Nrf2. Keap1/Nrf2$^{+/+}$ (n=15); Keap1$^{R554Q/+}$
644 (n=7); Keap1$^{R554Q/R554Q}$ (n=18); Nrf2$^{D29H/+}$ (n=18). Ns= not significant (Log-rank (Mantel-Cox) test). **B,**
645 Lung tumor-free survival of p53$^{fl/fl}$ mice expressing wild-type or mutant Keap1/Nrf2. Keap1/Nrf2$^{+/+}$ (n=11);
646 Keap1$^{R554Q/+}$ (n=6); Keap1$^{R554Q/R554Q}$ (n=16); Nrf2$^{D29H/+}$ (n=10). **C.** Representative H&E of mouse lung

647 depicting bronchiolar and alveolar cells of the p53$^{fl/fl}$ models (scale bars = 100μM (top panel), 20μM
648 (middle panel), 10μM (bottom panel)). **D,** Overall survival of Lkb1$^{fl/fl}$ mice expressing wild-type or mutant
649 Keap1/Nrf2. Keap1/Nrf2$^{+/+}$ (n=11); Keap1$^{R554Q/+}$ (n=7); Keap1$^{R554Q/R554Q}$ (n=11); Nrf2$^{D29H/+}$ (n=5). Ns= not
650 significant (Log-rank (Mantel-Cox) test). **E,** Lung tumor-free survival of Lkb1$^{fl/fl}$ mice expressing wild-type
651 or mutant Keap1/Nrf2. Keap1/Nrf2$^{+/+}$ (n=11); Keap1$^{R554Q/+}$ (n=6); Keap1$^{R554Q/R554Q}$ (n=9); Nrf2$^{D29H/+}$ (n=4).
652 **F,** Representative H&E of mouse lung depicting bronchiolar and alveolar cells of the Lkb1$^{fl/fl}$ models (scale
653 bars = 100μM (top panel), 20μM (middle panel), 10μM (bottom panel)). For **A, B, D, E,** mice were infected
654 intranasally with adenoviral-Cre, followed by collection at 500 days to analyze lung tissue histology.

655 **Figure 4.**

656 Keap1/Nrf2 mutation cooperates with Kras$^{G12D/+}$ to promote lung tumor initiation and early progression. **A,**
657 Overall survival of Keap1 mutant mice with Kras$^{G12D/+}$ mutation. Keap1$^{+/+}$ (n=16); Keap1$^{R554Q/+}$ (n=18);
658 Keap1$^{R554Q/R554Q}$ (n=18). **B,** Overall survival of Nrf2 mutant mice with Kras$^{G12D/+}$ mutation. Nrf2$^{+/+}$ (n=14);
659 Nrf2$^{D29H/+}$ (n=12). Ns = not significant (Log-rank (Mantel-Cox) test). **C,** Representative
660 immunohistochemical (IHC) staining of Nrf2 in Keap1/Nrf2 mutant tumors with Kras$^{G12D/+}$ mutation (scale
661 bars = 20 μM). **D,** H-scores for Nrf2 (nuclear) IHC staining. **E,** Representative immunohistochemical (IHC)
662 staining of Nrf2 target Nqo1 (scale bars = 20 μM). **F,** H-scores for Nqo1 (whole cell) IHC staining. For **C-**
663 **F**, N=3 mice per genotype and >20,000 tumor cells per mouse. *p<0.05 (one-way ANOVA). **G,**
664 Representative whole lung H&E-stained section (scale bars = 2000 μM). **H,** Tumor number per mouse in
665 Keap1/Nrf2 mutant models normalized to lung area. *p<0.05 (one-way ANOVA). **I,** Distribution of tumor
666 grades across Keap1/Nrf2 mutant models. *p<0.05 (unpaired t test with Holm-Sidak's multiple
667 comparisons test). AAH = atypical adenomatous hyperplasia. BH = bronchiolar hyperplasia. **J,** Fraction of
668 lung tumor burden by grade (lung tumor area/ total lung area per grade). *p<0.05 (unpaired t test with
669 Holm-Sidak's multiple comparisons test). For both **I** and **J** n=10 mice and ≥2,000 tumors per genotype.

670 **Figure 5.**

671 Homozygous Keap1$^{R554Q}$ impairs adenocarcinoma progression in the Kras$^{G12D/+}$; p53$^{fl/fl}$ model. **A,** Overall
672 survival of Kras$^{G12D/+}$; p53$^{fl/fl}$ mice with Keap1 mutation. Keap1$^{+/+}$ (n=20); Keap1$^{R554Q/+}$ (n=11);
673 Keap1$^{R554Q/R554Q}$ (n=25). **B,** Overall survival of Kras$^{G12D/+}$; p53$^{fl/fl}$ mice with Nrf2 mutation. Nrf2$^{+/+}$ (n=25);

674 Nrf2$^{D29H/+}$ (n=29). Ns = not significant (Log-rank (Mantel-Cox) test). **C,** Representative
675 immunohistochemical (IHC) staining of Nrf2 in Kras$^{G12D/+}$; p53$^{fl/fl}$ mice with Keap1/Nrf2 mutation (scale
676 bars = 20 μM). **D,** H-scores for Nrf2 (nuclear) IHC staining. **E,** Representative immunohistochemical (IHC)
677 staining of Nrf2 target Nqo1 (scale bars = 20 μM). **F,** H-scores for Nqo1 (whole cell) IHC staining. For **C-**
678 **F**, N=3 mice per genotype and >20,000 tumor cells per mouse. *p<0.05 (one-way ANOVA). **G,**
679 Representative whole lung H&E stained section (scale bars = 2000 μM). **H,** Distribution of tumor grades
680 across Keap1/Nrf2 mutant models. *p<0.05 (unpaired t test with Holm-Sidak's multiple comparisons test).
681 $ = fewer than 3 tumors detected across all mice. **I,** Fraction of lung tumor burden by grade (lung tumor
682 area per grade/ total lung area). *p<0.05 (unpaired t test with Holm-Sidak's multiple comparisons test). $
683 = fewer than 3 tumors detected across all mice. For both **H** and **I** n≥9 mice and ≥1,900 tumors per
684 genotype. Only one grade 5 tumor was found in the Keap1$^{R554Q/R554Q}$ cohort, and therefore was excluded
685 from these analyses.

686 **Figure 6.**

687 Nrf2 expression and activity is reduced in higher-grade tumors. **A,** Representative Nrf2 and Nqo1 IHC
688 staining in grade 1 and 4 tumors from Kras$^{G12D/+}$; p53$^{fl/fl}$ mice with Keap1 or Nrf2 mutation (scale bars = 20
689 μM). **B, C** Heatmaps depicting the H-scores per grade from IHC staining for Nrf2 (nuclear) **(B)**, and the
690 Nrf2 target Nqo1 (whole cell) **(C)**. N=3 mice per genotype, >20,000 tumor cells per mouse. Only one
691 grade 5 tumor was found in the Keap1$^{R554Q/R554Q}$ cohort, and therefore was excluded from these analyses.

692 **Figure 7.**

693 NRF2 overexpression impairs lung cancer cell proliferation, viability, and soft agar colony formation. **A,**
694 Dependency scores obtained from DepMap(45) and represented as *NFEL2* 22Q2 Public+Score, Chronos
695 for NSCLC cell lines previously determined to have high or low NRF2 activity(24). NRF2 mutant line
696 symbols are represented by yellow, KEAP1 mutant lines by dark red or dark blue, and KEAP1 deleted
697 lines by green. ***p<0.0001 (unpaired t-test). **B,** Western blot analysis of NRF2, β-actin, and NRF2 target
698 GCLC, xCT, and GSR expression in *KEAP1* mutant lung cancer cell lines transduced with PLX317-empty
699 vector (EV) or PLX317-NRF2 (NRF2). **C,** Representative images of HCC15 cells transduced with EV or
700 NRF2 demonstrating cell confluency (enhanced contour) and cell death (Sytox Green) (scale bars = 100

701 μM). **D, E,** Analysis of EV and NRF2 HCC15 cell proliferation and death over 96 hours. Proliferation is
702 represented as % confluency at each time point, and cell death as the number of Sytox Green positive
703 cells per area normalized to % confluency. N=3 technical replicates per cell line, and two independent
704 experiments. **F, G,** Area under the curve (AUC) analysis of cell proliferation **(F)** and Sytox Green-positive
705 cell death **(G)** in KEAP1 mutant lung cancer cells lines +/- NRF2, normalized to empty vector control.
706 *p<0.05 (one-way ANOVA). For **C-G** NSCLC cells were seeded in triplicate in 96-well plates at a density
707 of 2,500 cells/ well. **H,** Representative images of H460 and HCC15 soft agar colony formation +/- NRF2. **I,**
708 Quantification of soft agar colony number of *KEAP1* mutant lung cancer cell lines. *p<0.05 (one-way
709 ANOVA). N=3 technical replicates per cell line, two independent experiments. For **H, I,** 5,000 cells per
710 well were seeded in 6-well plates in triplicate.

711 **Figure 8.**

712 Single copy Nrf2 deletion rescues homozygous Keap1$^{R554Q}$-mediated adenocarcinoma progression
713 impairment in the Kras$^{G12D/+}$; p53$^{fl/fl}$ model. **A,** Overall survival of Kras$^{G12D/+}$; p53$^{fl/fl}$ mice with Keap1
714 mutation and/ or single copy Nrf2 deletion. Keap1$^{+/+}$; Nrf2$^{+/+}$ (n=16), Keap1$^{+/+}$; Nrf2$^{fl/+}$ (n=7),
715 Keap1$^{R554Q/R554Q}$; Nrf2$^{+/+}$ (n=10), Keap1$^{R554Q/R554Q}$; Nrf2$^{fl/+}$ (n=11). Ns = not significant (Log-rank (Mantel-
716 Cox) test). **B,** Representative immunohistochemical (IHC) staining of Nrf2 in Kras$^{G12D/+}$; p53$^{fl/fl}$ mice with
717 Keap1 mutation and/ or heterozygous Nrf2 deletion (scale bars = 20 μM). **C,** H-scores for Nrf2 (nuclear)
718 IHC staining. **D,** Representative IHC staining of Nrf2 target Nqo1 (scale bars = 20 μM). **E,** H-scores for
719 Nqo1 (whole-cell) IHC staining. For **B-E**, N=3 mice per genotype and >20,000 tumor cells per mouse.
720 *p<0.05 (one-way ANOVA). **F,** Representative whole lung H&E-stained sections (scale bars = 2000 μM).
721 **G,** Distribution of tumor grades across Keap1 mutant/ Nrf2-deleted models. *p<0.05 (unpaired t test with
722 Holm-Sidak's multiple comparisons test). $ = fewer than 3 tumors detected across all mice. **H,** Fraction of
723 lung tumor burden by grade (lung tumor area per grade/ total lung area). *p<0.05 (unpaired t test with
724 Holm-Sidak's multiple comparisons test). $ = fewer than 3 tumors detected across all mice. For both **G**
725 and **H** n=7 mice and ≥1,000 tumors per genotype were analyzed. Only one grade 4 and one grade 5
726 tumor were found in the Keap1$^{R554Q/R554Q}$ cohort, and therefore were excluded from these analyses.

727

728 **Online supplemental material**

729 Supplementary Fig. S1 shows that the *CA-Keap1*$^{R554Q}$ allele does not exhibit hypomorphism in mouse
730 embryonic fibroblasts. Supplementary Fig. S2 shows lung tumor analysis data for Keap1/Nrf2 mutant
731 mice in the Kras$^{G12D/+}$ model. Supplementary Fig. S3 shows lung tumor analysis data and tumor cell
732 proliferation/ death immunohistochemical staining for Keap1/Nrf2 mutant mice in the Kras$^{G12D/+}$; p53$^{fl/fl}$
733 model. Supplementary Fig. S4 shows the H-scores by tumor grade of Nrf2 and Nqo1
734 immunohistochemical staining in Kras$^{G12D/+}$; p53$^{fl/fl}$ and Kras$^{G12D/+}$; p53$^{fl/fl}$; Keap1$^{R554Q/R554Q}$ mouse models
735 with single copy Nrf2 deletion. Supplementary Fig. S5 shows lung tumor analysis data in the Kras$^{G12D/+}$;
736 p53$^{fl/fl}$ model with single copy Nrf2 deletion.

737

738 **Author Contributions**

739 G.M.D. conceived the project and G.M.D. and J.M.D. designed the experiments. G.M.D., I.I.C.C. and
740 F.A.K. designed and generated the Nrf2 and Keap1 mutant mice. G.M.D. performed the RNA
741 sequencing. Maintenance of animal colonies, generation of experimental animals, and collections of
742 tissues were performed by A.F., with assistance from S.C. and N.F.P. J.M.D. performed cell line
743 experiments, immunohistochemistry, and tumor histology analyses. J.R.P. and E.E.S. generated the
744 affinity-purified NRF2 antibody used for immunohistochemistry. J.M.D. and G.M.D. wrote the manuscript,
745 and all authors reviewed it. G.M.D. acquired funding and supervised the study.

746

747

Figure 1.

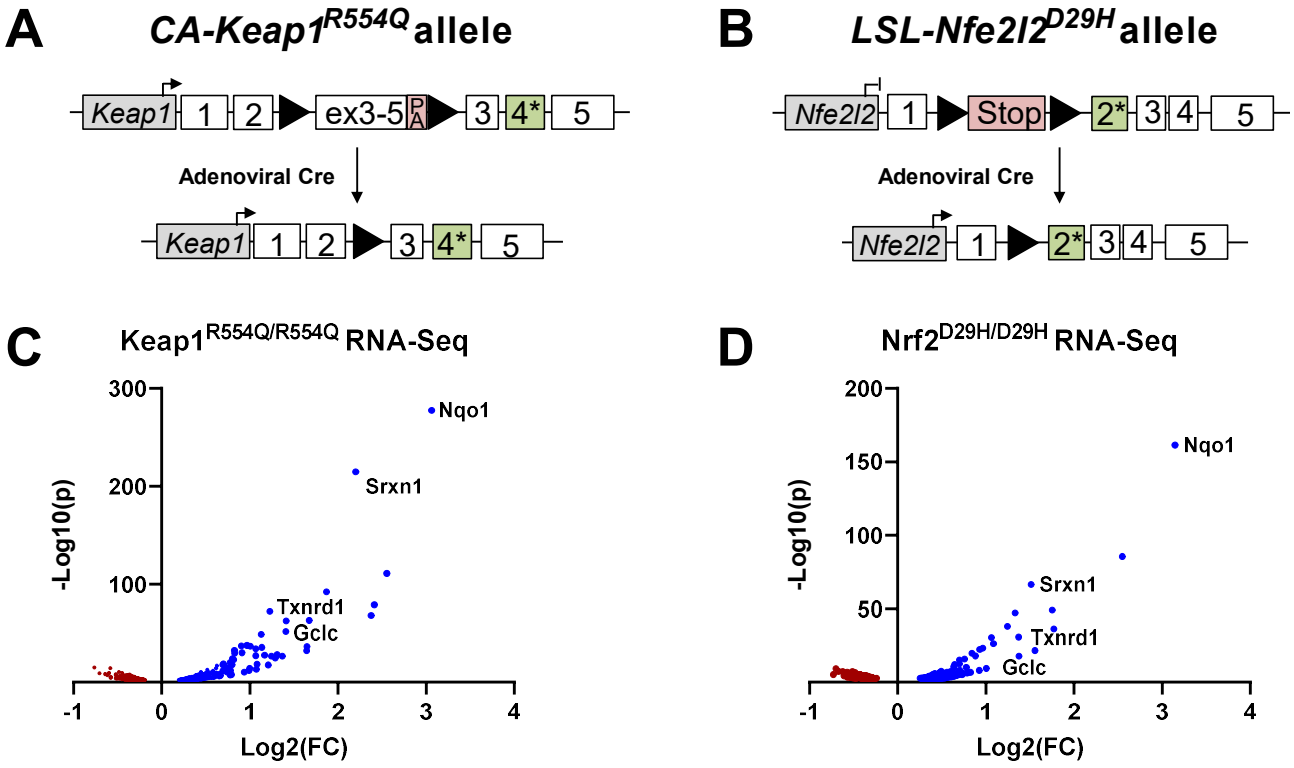
A
CA-Keap1R554Q allele
Keap1
1
2
ex3-5
PA
3
4*
5
Adenoviral Cre
Keap1
1
2
3
4*
5
B
LSL-Nfe2l2D29H allele
Nfe2l2
1
Stop
2*
3
4
5
Adenoviral Cre
Nfe2l2
1
2*
3
4
5
C
Keap1R554Q/R554Q RNA-Seq
-Log10(p)
Log2(FC)
Nqo1
Srxn1
Txnrd1
Gclc
D
Nrf2D29H/D29H RNA-Seq
-Log10(p)
Log2(FC)
Nqo1
Srxn1
Txnrd1
Gclc

Figure 2.

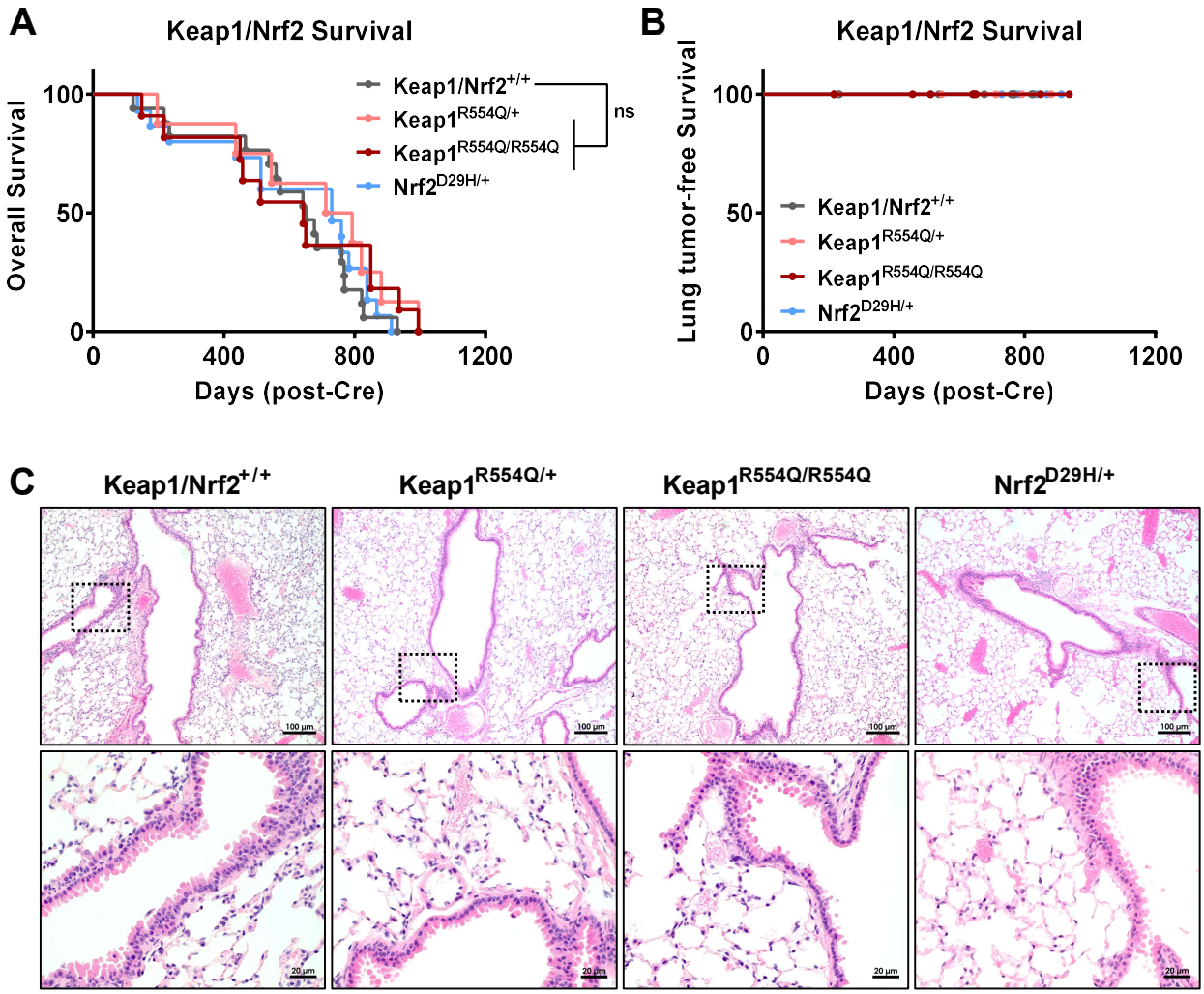
A
Keap1/Nrf2 Survival
Overall Survival
100
50
0
0
400
800
1200
Days (post-Cre)
Keap1/Nrf2+/+
Keap1R554Q/+
Keap1R554Q/R554Q
Nrf2D29H/+
ns
B
Keap1/Nrf2 Survival
Lung tumor-free Survival
100
50
0
0
400
800
1200
Days (post-Cre)
Keap1/Nrf2+/+
Keap1R554Q/+
Keap1R554Q/R554Q
Nrf2D29H/+
C
Keap1/Nrf2+/+
Keap1R554Q/+
Keap1R554Q/R554Q
Nrf2D29H/+
100 µm
20 µm

Figure 3.

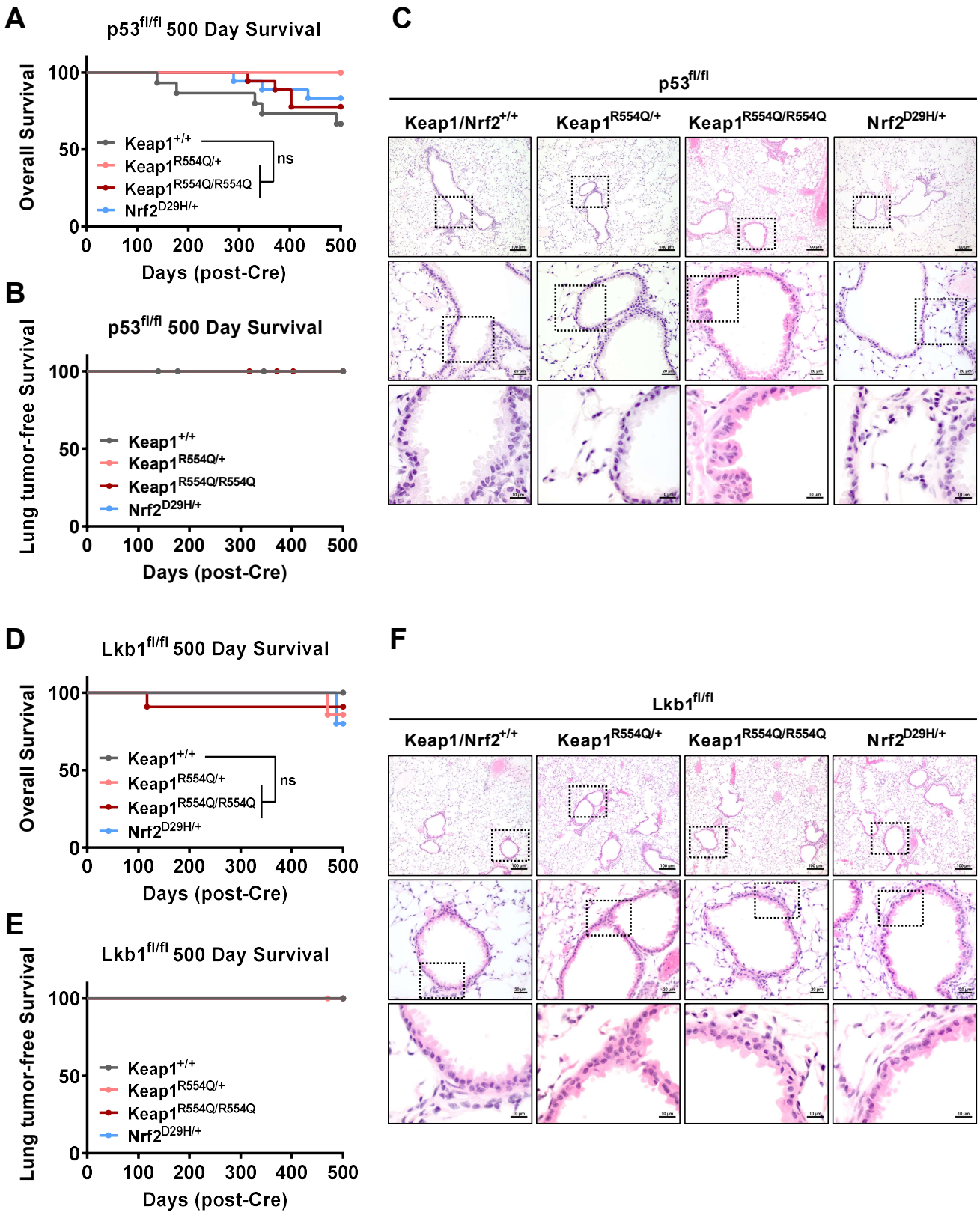
A
p53fl/fl 500 Day Survival
Overall Survival
100
50
0
0
100
200
300
400
500
Days (post-Cre)
Keap1+/+
Keap1R554Q/+
Keap1R554Q/R554Q
Nrf2D29H/+
ns
B
p53fl/fl 500 Day Survival
Lung tumor-free Survival
Days (post-Cre)
C
p53fl/fl
Keap1/Nrf2+/+
Keap1R554Q/+
Keap1R554Q/R554Q
Nrf2D29H/+
D
Lkb1fl/fl 500 Day Survival
Overall Survival
Days (post-Cre)
E
Lkb1fl/fl 500 Day Survival
Lung tumor-free Survival
Days (post-Cre)
F
Lkb1fl/fl
Keap1/Nrf2+/+
Keap1R554Q/+
Keap1R554Q/R554Q
Nrf2D29H/+

Figure 4.

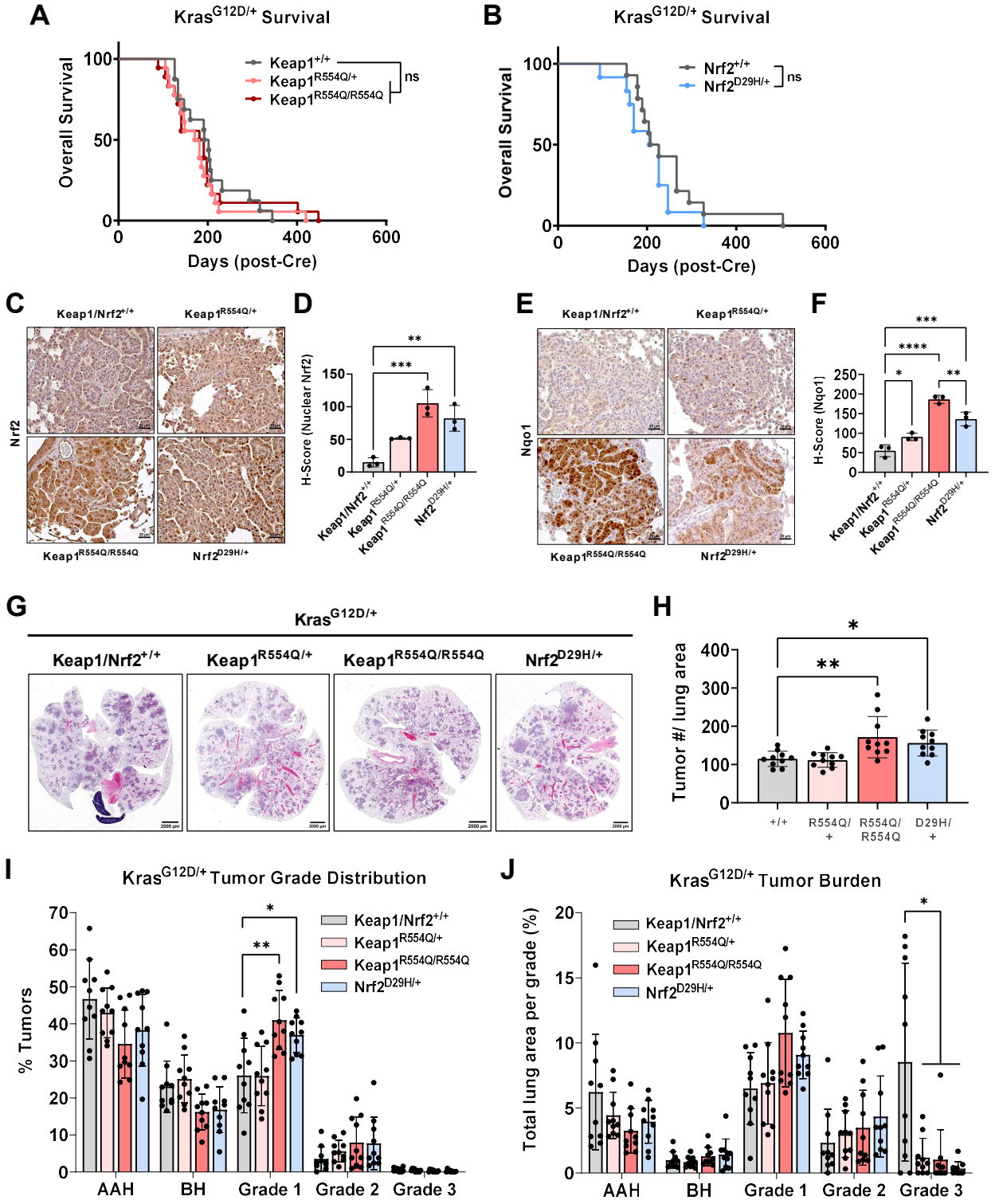
A
KrasG12D/+ Survival
Overall Survival
Days (post-Cre)
Keap1+/+
Keap1R554Q/+
Keap1R554Q/R554Q
ns
B
KrasG12D/+ Survival
Nrf2+/+
Nrf2D29H/+
ns
C
Keap1/Nrf2+/+
Keap1R554Q/+
Nrf2
Keap1R554Q/R554Q
Nrf2D29H/+
D
H-Score (Nuclear Nrf2)
E
Keap1/Nrf2+/+
Keap1R554Q/+
Nqo1
Keap1R554Q/R554Q
Nrf2D29H/+
F
H-Score (Nqo1)
G
KrasG12D/+
Keap1/Nrf2+/+
Keap1R554Q/+
Keap1R554Q/R554Q
Nrf2D29H/+
H
Tumor #/ lung area
+/+
R554Q/+
R554Q/R554Q
D29H/+
I
KrasG12D/+ Tumor Grade Distribution
% Tumors
AAH
BH
Grade 1
Grade 2
Grade 3
J
KrasG12D/+ Tumor Burden
Total lung area per grade (%)

Figure 5.

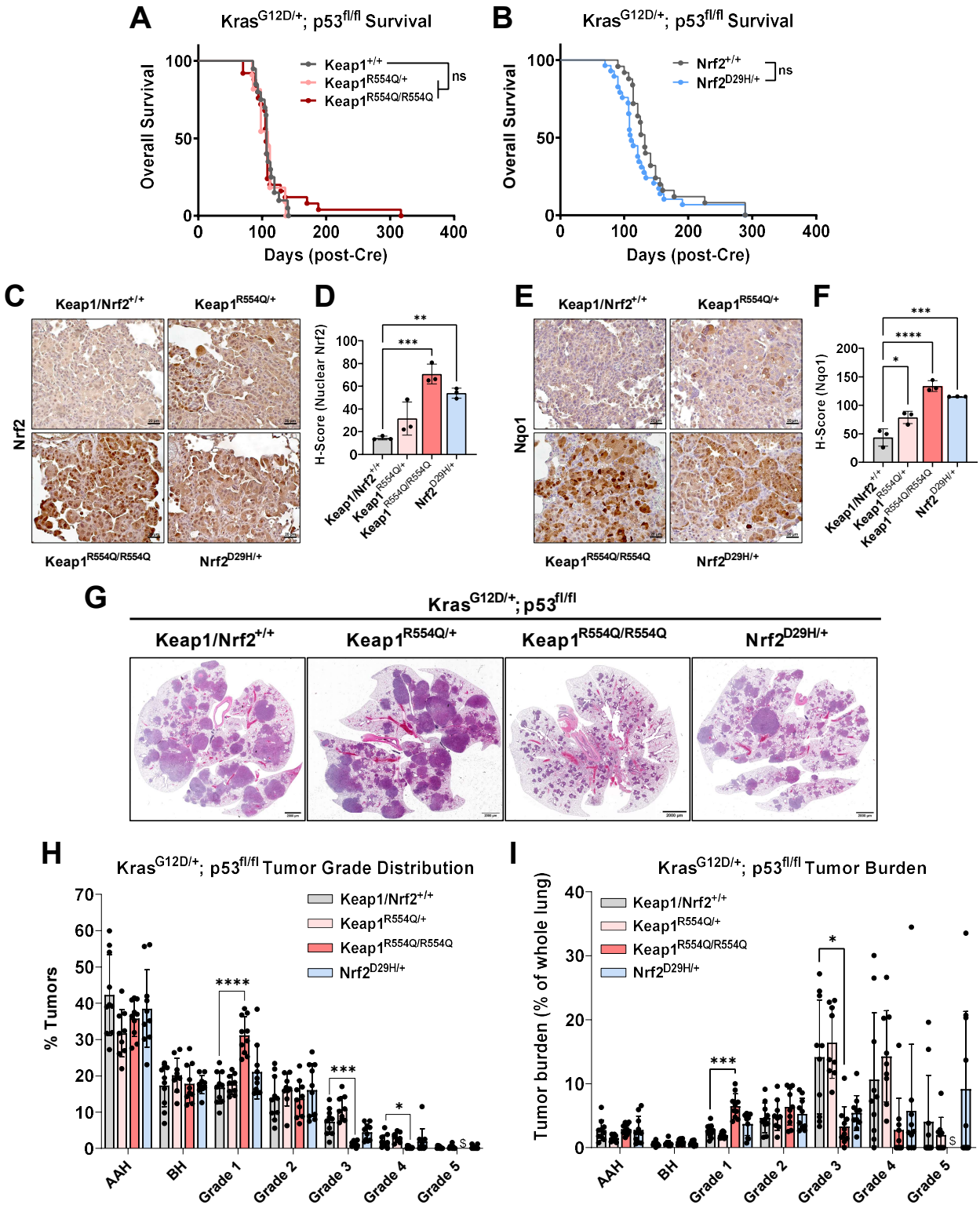
A
KrasG12D/+; p53fl/fl Survival
Overall Survival
Days (post-Cre)
Keap1+/+
Keap1R554Q/+
Keap1R554Q/R554Q
ns
B
KrasG12D/+; p53fl/fl Survival
Nrf2+/+
Nrf2D29H/+
C
Keap1/Nrf2+/+
Keap1R554Q/+
Nrf2
Keap1R554Q/R554Q
Nrf2D29H/+
D
H-Score (Nuclear Nrf2)
E
Nqo1
F
H-Score (Nqo1)
G
KrasG12D/+; p53fl/fl
H
KrasG12D/+; p53fl/fl Tumor Grade Distribution
% Tumors
AAH
BH
Grade 1
Grade 2
Grade 3
Grade 4
Grade 5
I
KrasG12D/+; p53fl/fl Tumor Burden
Tumor burden (% of whole lung)

Figure 6.

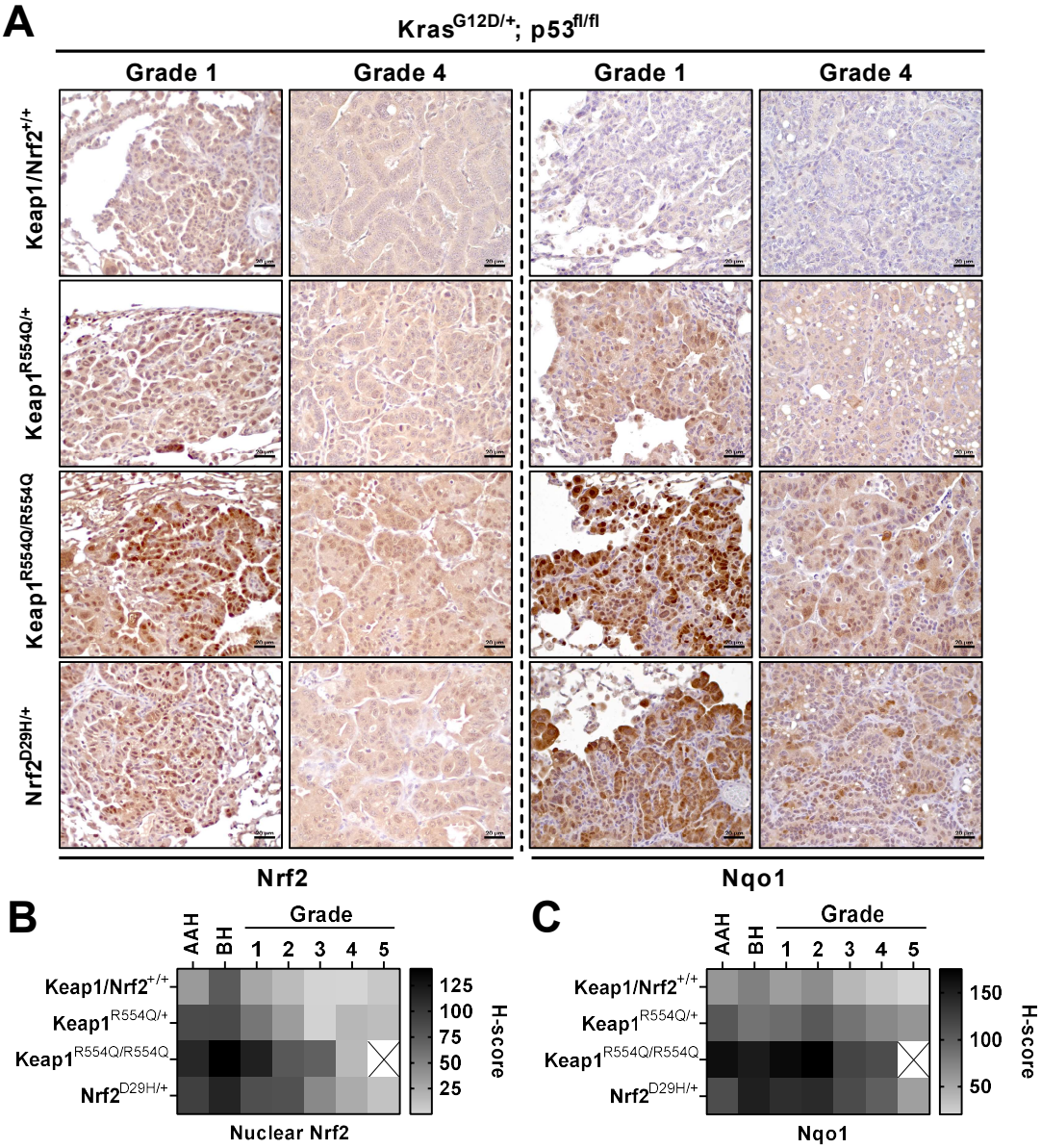
A
Kras$^{G12D/+}$; p53$^{fl/fl}$
Grade 1
Grade 4
Grade 1
Grade 4
Keap1/Nrf2$^{+/+}$
Keap1$^{R554Q/+}$
Keap1$^{R554Q/R554Q}$
Nrf2$^{D29H/+}$
Nrf2
Nqo1
B
AAH
BH
Grade
1 2 3 4 5
Keap1/Nrf2$^{+/+}$
Keap1$^{R554Q/+}$
Keap1$^{R554Q/R554Q}$
Nrf2$^{D29H/+}$
125
100
75
50
25
H-score
Nuclear Nrf2
C
AAH
BH
Grade
1 2 3 4 5
Keap1/Nrf2$^{+/+}$
Keap1$^{R554Q/+}$
Keap1$^{R554Q/R554Q}$
Nrf2$^{D29H/+}$
150
100
50
H-score
Nqo1

Figure 7.

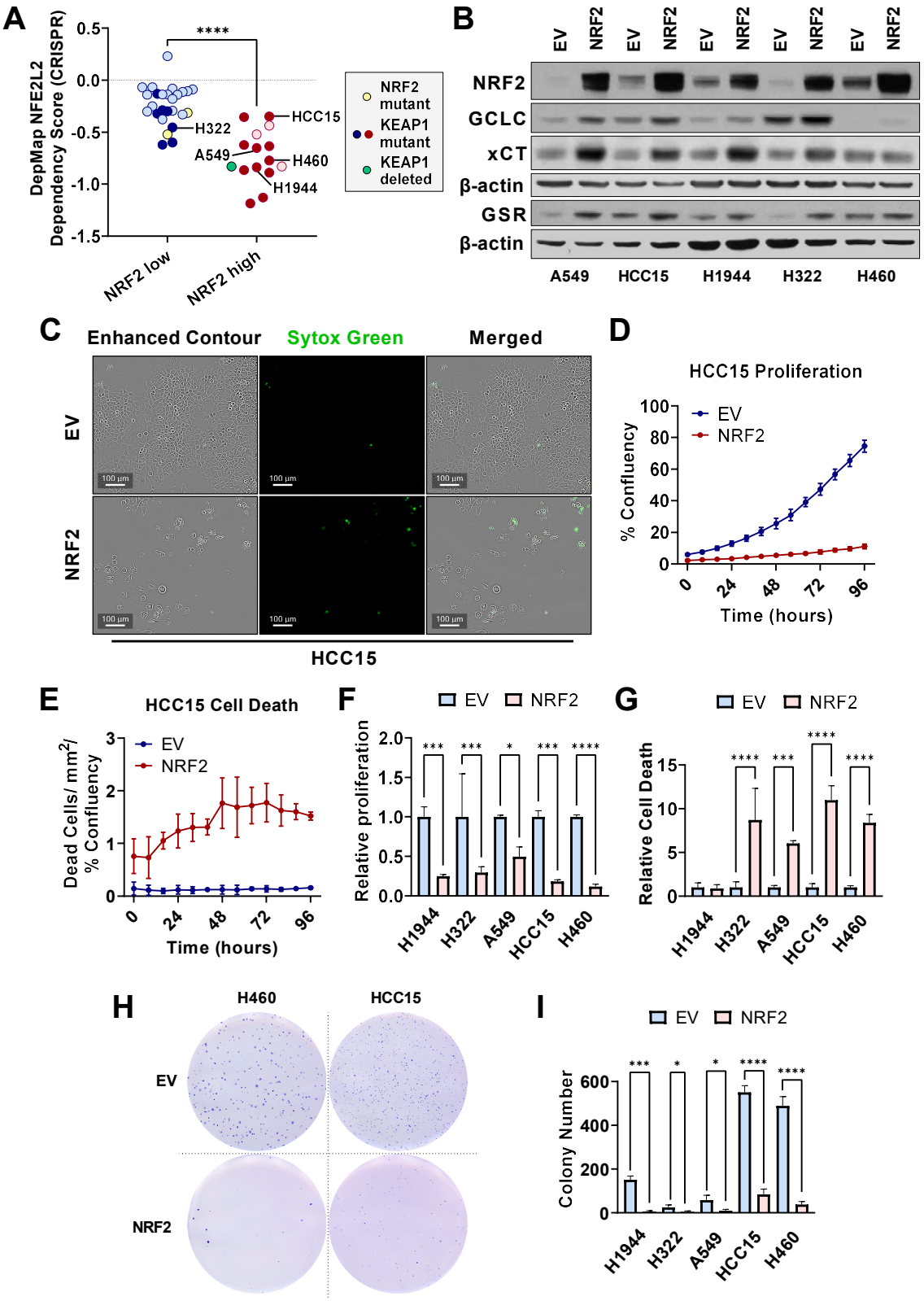
A
DepMap NFE2L2 Dependency Score (CRISPR)
****
HCC15
H322
A549
H460
H1944
NRF2 low
NRF2 high
NRF2 mutant
KEAP1 mutant
KEAP1 deleted
B
EV
NRF2
NRF2
GCLC
xCT
β-actin
GSR
β-actin
A549
HCC15
H1944
H322
H460
C
Enhanced Contour
Sytox Green
Merged
EV
NRF2
HCC15
D
HCC15 Proliferation
% Confluency
Time (hours)
E
HCC15 Cell Death
Dead Cells/ mm²/ % Confluency
Time (hours)
F
Relative proliferation
G
Relative Cell Death
H
H460
HCC15
EV
NRF2
I
Colony Number

Figure 8.

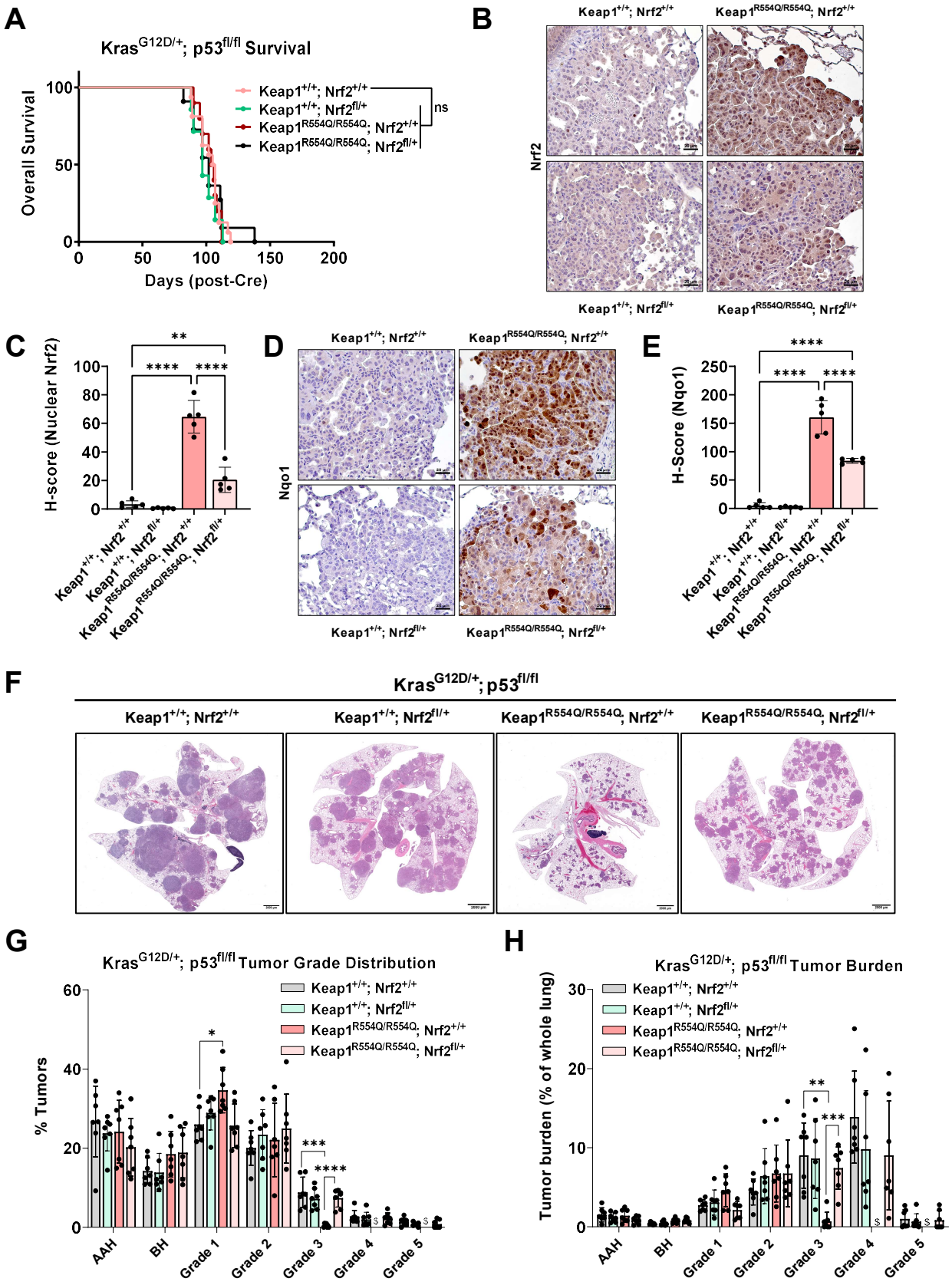
A
Kras$^{G12D/+}$; p53$^{fl/fl}$ Survival
Overall Survival
Days (post-Cre)
Keap1$^{+/+}$; Nrf2$^{+/+}$
Keap1$^{+/+}$; Nrf2$^{fl/+}$
Keap1$^{R554Q/R554Q}$; Nrf2$^{+/+}$
Keap1$^{R554Q/R554Q}$; Nrf2$^{fl/+}$
ns
B
Nrf2
C
H-score (Nuclear Nrf2)
D
Nqo1
E
H-Score (Nqo1)
F
Kras$^{G12D/+}$; p53$^{fl/fl}$
G
Kras$^{G12D/+}$; p53$^{fl/fl}$ Tumor Grade Distribution
% Tumors
AAH
BH
Grade 1
Grade 2
Grade 3
Grade 4
Grade 5
H
Kras$^{G12D/+}$; p53$^{fl/fl}$ Tumor Burden
Tumor burden (% of whole lung)